Effects of viscosity and conductivity stratification on the linear stability and transient growth within compressible Couette flow

Bijaylakshmi Saikia, Ashwin Ramachandran, and Krishnendu Sinha,*

Indian Institute of Technology Bombay, Mumbai, 400076, India

Rama Govindarajan

International Centre for Theoretical Sciences, Bengaluru, 560089, India

Abstract

Accurate prediction of laminar to turbulent transition in compressible flows is a challenging task, as it can be affected by a combination of factors. Compressibility causes large variations in thermodynamic as well as transport properties of a gas, which in turn are known to affect flow stability. We study the stratification of individual transport properties, and their combined behavior. We also examine the effect of change in the magnitude of viscosity and conductivity on flow stability. The Couette flow of a perfect gas is our model problem and both modal and non-modal analyses are carried out. We notice a large destabilizing role of increase in the conductivity value and a dramatic stabilizing effect of mean viscosity stratification, over a range of free-stream Mach number, Reynolds number, Prandtl number and disturbance wavenumber. In the combined case, the viscosity stratification plays a dominant role. We find this to be the case for finite-time transient growth in the parameter regime below linear instability as well as asymptotically at large time. A budget of the transient growth energy amplification is also shown to identify the effects of transport properties on the constituents of perturbation energy. The extensive results presented in this paper, we believe should motivate those studying more realistic flows to examine how these contrasting effects of stratification come together.

Keywords: Transition, high-speed flows, transport property, Prandtl number, energy budget.

* krish@aero.iitb.ac.in

I. INTRODUCTION

A good prediction of boundary layer transition from laminar to turbulent flow is an important concern due to its influence on surface heat flux, skin-friction drag and flow-separation characteristics. The transition process can be affected by a wide range of factors [1]-[5]. For example, receptivity to free-stream turbulence/entropy/vortical disturbances, surface curvature, angle of attack and nose bluntness can alter the transition location significantly. In addition, boundary conditions imposed on the vehicle surface, such as, cold/adiabatic, smooth/rough, catalytic/non-catalytic can delay or augment the transition process. The variation in thermodynamic and transport properties of the gas can also have a major influence on flow stability [6]-[7]. In the context of drag reduction, the role of transport property variation, mainly that of viscosity stratification, has been studied widely for incompressible as well as non-Newtonian flows and is well documented in Ref. [8]-[18].

To demonstrate the destabilizing role of viscosity stratification, Yih [8] considers a plane Couette-Poiseuille flow of two superposed layers of fluids with different viscosities. He finds that if the viscosity varies between the layers, and the depth ratio and the viscosity ratio are within certain ranges, both plane Poiseuille and Couette flow can be unstable at any Reynolds number. In the case of incompressible boundary layers, Wall and Wilson [9] examine the effect of different viscosity models on flow stability and notice that a non-uniform decrease in viscosity across the boundary layer stabilizes the flow and the extent of stabilization increases as Prandtl number is increased. To investigate the role of variation of thermal conductivity on flow stability, Sorokin [10] studies a vertical plane fluid layer with thermal conductivity depending linearly on temperature. He observes that relatively small changes in the thermal conductivity caused by a variation in temperature results in flow destabilization.

The crucial role of continuous viscosity stratification at the critical layer, where the phase velocity of the disturbance coincides with the mean flow velocity, is first realized by Craik [11] for a plane Couette flow. Ranganathan and Govindarajan [12] study a channel flow of two fluids of different viscosities with a mixed layer in between, and find that an overlap of the critical layer with the layer of viscosity stratification leads to an order of magnitude stabilization of the flow. This stabilization is attributed to the reduction in energy intake from the mean flow to the disturbance in Ref. [13]. Govindarajan et al. in Ref. [14] observe

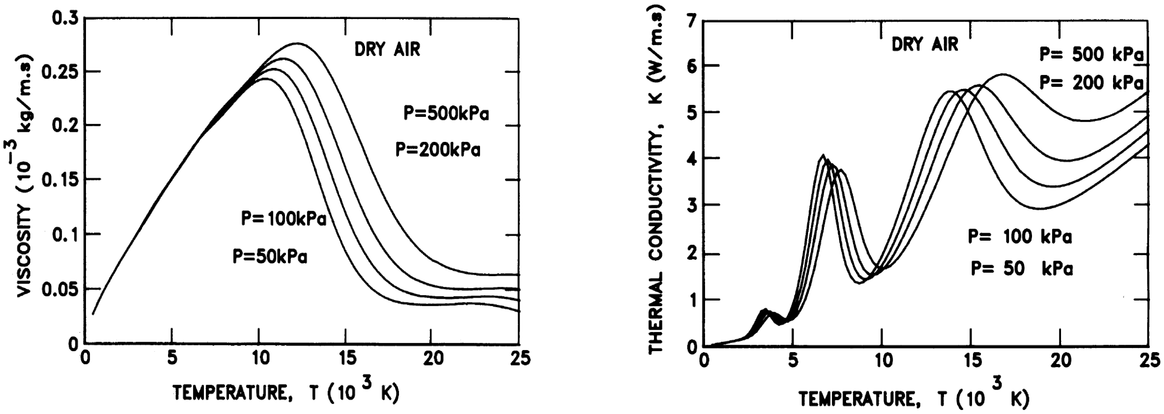

(a) Viscosity

(b) Thermal conductivity

FIG. 1: Variation of viscosity and thermal conductivity with pressure and temperature for equilibrium air. Reprinted with permission from M. I. Boulos, P. Fauchais, and E. Pfender, Thermal Plasmas (Springer, New York, 1994), Copyright 2004, Springer [19].

that the exact form of the viscosity profile is immaterial; any monotonic continuous profile of viscosity in the thin mixed layer gives the same answer. In Ref. [15], Govindarajan finds that for a channel flow with two fluids of high mass diffusivity, a new mode of instability (overlap mode) appears, when the critical layer of the dominant disturbance overlaps the viscosity stratified layer.

The role of viscosity stratification on transient energy growth of the disturbances have also been studied for incompressible flows. Chikkadi et al. [16] notice that transient growth of disturbances, including that of the streamwise vortices, are practically unaffected by viscosity stratification. Sameen and Govindarajan [17] also observe similar effect of viscosity stratification alone, but they notice that increasing the relative magnitudes of momentum to thermal diffusivity i.e., the Prandtl number, transient growth increases dramatically. Nouar et al. [18] revisit a few previous studies related to the stability of viscosity stratified channel flow, and conclude that for Carreau fluids, transition is effectively postponed when a viscosity contrast is produced in the critical layer.

In the case of compressible flows, it is well known that the coupling between the momentum and energy equations leads to the existence of multiple instability modes, as opposed to the single instability mode (Tollmien-Schlichting mode) of incompressible flows. Moreover, the same factors which act to stabilize the incompressible flow, can have a destabilizing effect for compressible flows. For example, wall cooling is found to stabilize the first instability mode, but it strongly destabilizes the second mode, which is dominant at high Mach numbers.

In the case of high-speed flows, large changes in pressure, density, temperature and gas composition, in the presence of chemical reactions, can lead to a large variation in the transport properties of the gas. The Sutherland's formula with a fixed value of Prandtl number is standardly used to compute the transport properties, such that the variations in viscosity and thermal conductivity are coupled. More realistic estimates of transport properties, especially in high-Mach number applications, can be obtained using Blottner curve-fits with mixing rule or collision cross-section based formulations. Viscosity and conductivity data for air as a function of pressure and temperature (Fig. 1) shows large non-monotonic variation, which leads to a significant change in the effective Prandtl number. Further, the variation of transport properties and the resulting effect on flow instabilities, are dependent on the specific transport model used. The problem is exacerbated by the fact that stability results are often very sensitive to minute changes in the flow properties. This is a major disadvantage in studying the stability characteristics of high-speed flows, especially in the absence of an universally accepted transport model.

Stability studies of high-speed flows have reported that transport property effects can dominate over other thermodynamic and chemical reaction rate variations. Lyttle and Reed [7] consider a spherically blunted right circular cone at a Mach number of 13.5, and investigate the sensitivity of two different transport models (Stuckert and Blottner) on the second mode growth rate. They find that the peak growth rate of the second mode changes by around 8%, due to a 10% and 25% change in the viscosity and thermal conductivity values respectively. Franko et al. [6] consider a flat plate geometry at a Mach number of 10, and investigate the effect of using different chemistry models for thermodynamic, transport and chemical reactions on boundary layer stability. They report a 20% difference in the peak growth of the second mode, between the two transport models (Blottner and Chapman-Enskog method).

A significant amount of work has also been carried out to investigate the physical effect of transport properties on the stability of compressible flows. Using linear stability theory, Hu and Zhong [20] study the effect of viscosity on the first even and odd acoustic modes, by comparing the viscous results at finite Reynolds numbers with the inviscid results of Duck et al. [21]. They observe that viscosity can destabilize these modes for certain combinations of

Reynolds number and wave number. To study the effect of stratification in viscosity, Malik et al. [22] compare their work on uniform viscosity Couette flow, with the stratified viscosity results of Hu and Zhong [20]. They notice that the gradient in viscosity has a profound stabilizing effect and it increases the critical Reynolds number of the flow significantly. However, a constant Prandtl number is assumed in these studies, which implies that viscosity and thermal conductivity are proportional and they vary together. This is often not the case in high-Mach number flows, where the transport properties have large independent variations with temperature and pressure (see Fig. 1). The current work investigates the effect of such variations in conductivity and viscosity on the flow stability at high-Mach number.

The objective of our work is to understand separately the effects of viscosity, conductivity and their stratification on the stability of high-speed flows. In realistic flows, the variations of different transport properties are usually related to other effects of chemical reactions and internal energy excitation. The effect on stability is therefore due to a combination of multiple effects and it is difficult to know which one is responsible for a particular trend. There can also be competing effects, which can change from one flow configuration to another. In this paper, we perform controlled studies with variation of individual transport properties to bring out the underlying physical effects. Combined and coupled variation of viscosity and conductivity are also considered to understand how they come together. We suppress high-temperature effects, like chemical reactions and vibrational relaxation, and assume a perfect gas flow, so as to focus on transport property variations and their effect on flow stability. Non-equilibrium thermo-chemistry effect on flow stability have been studied earlier, for example, Malik & Anderson [23], Hudson et al. [24] and others.

In this work, we have a chosen Couette flow to study the stability of stratified viscosity and conductivity flows, and compare it with that of flows with uniform transport properties. This flow has the advantage that geometry effects are kept to a minimum, and the shear is constant. Indeed, the stability of stratified flows in simple geometries, like Couette and Poiseuille, has been studied extensively in the literature since the classical work of Yih [8]. A reference flow is taken in which viscosity and conductivity are held constant at their respective reference values (typically, at the top-wall reference temperature). Two other flows are also considered – one with viscosity varying with temperature across the shear layer, keeping conductivity constant; and the other with uniform viscosity, but conductivity varying with temperature. We consider one more model problem where both viscosity and conductivity vary together in a coupled way, and the stability results for this case are compared with those mentioned above as well as the reference flow with uniform transport properties.

We perform a linear stability analysis to investigate the most unstable modes for all the model problems considered, and how they depend on Mach, Reynolds and disturbance wave numbers. The dominant growth rates and critical Reynolds numbers are compared to isolate the effects of viscosity and conductivity variation in the flow. Linear stability analysis is useful where the transition process begins with the laminar flow going linearly unstable to disturbance modes for a small range of wave numbers. However, in some cases, the eigenspectrum may consist of decaying modes alone, but the disturbance energy can grow transiently to very high values and enable nonlinearities to emerge. Therefore we have also conducted a non-modal analysis to study the effect of the variation of transport properties on the transient energy growth of the disturbances. This will help us to identify any unstable region if exist, that was predicted as stable by the linear stability theory.

We note that the model problems presented above are theoretical constructs, specifically designed for the purpose outlined above. In real life, high-speed flows have myriad competing effects, and there is no way in an experiment to isolate each effect independently. Numerical experiments of the kind presented in this paper can prove to be a valuable tool and possibly the only way, to study and understand underlying physical effects. We also caution the reader that the present results are for the simplest of shear flows, namely a Couette flow, and not trivially extendable to other geometries. However, given that the transport properties in a realistic high-Mach number flow depend on temperature, pressure and composition in a non-trivial way, our findings about the individual effects of viscosity and conductivity could be of value to those studying more complex situations. We hope that these findings will motivate those working on more realistic compressible flows to examine whether transport property stratification can indeed be a source of destabilization.

II. BASE FLOW

The flow considered in this paper is a perfect Newtonian gas, confined between two parallel plates, with the upper plate moving with a velocity of U_∞ and the lower wall is at rest. The distance between the two plates and the upper wall quantities are used to non-dimensionalize the flow variables. The assumption of steady and unidirectional flow, simplifies the base flow equations to the following form:

x **momentum:**

$$\frac{\partial}{\partial y}(\bar{\mu}\frac{\partial \bar{U}}{\partial y}) = 0, \tag{1}$$

energy equation:

$$\frac{\partial}{\partial y}(\bar{\kappa}\frac{\partial \bar{T}}{\partial y}) + (\gamma - 1)\, M^2\, Pr\, \bar{\mu}\, (\frac{\partial \bar{U}}{\partial y})^2 = 0. \tag{2}$$

Here U, T, μ, κ and γ represent streamwise velocity, temperature, viscosity, thermal conductivity and the ratio of specific heats respectively; y denotes the wall-normal direction. The reference Prandtl number, Mach number and Reynolds number are defined in terms of the top wall conditions and are denoted by Pr, M and Re respectively. The overbar is used to indicate the non-dimensionalized mean flow quantities. Velocity satisfies the no-slip condition at both the walls. The temperature boundary conditions imposed on the upper and lower walls are isothermal and adiabatic respectively.

To examine the physical effects of viscosity and thermal conductivity, we have considered three different model problems. These are – stratified viscosity flow, stratified conductivity flow and stratified viscosity and conductivity flow, and we denote them as μ-stratified, κ-stratified and μ-κ-stratified flow, respectively. In a μ-stratified flow, only the variation of viscosity is allowed, and conductivity is kept at its reference value. In a κ-stratified flow, the conductivity varies as a function of temperature, and viscosity is maintained at its reference value. A μ-κ-stratified flow allows the variation of viscosity and thermal conductivity simultaneously, as a function of temperature. We use Sutherland's law for air to compute viscosity and conductivity at varying temperature. It is consistent with the current framework of compressible flow of a perfect gas, without any high-temperature effects like dissociation and ionization.

A. κ-stratified flow

In a κ-stratified flow, since the viscosity is maintained at its reference value (= 1), the base flow velocity varies linearly as the wall-normal distance ($\bar{U} = y$). The thermal conductivity is varied using the Sutherland's formula (Eq. 3), where T_{ref} denotes the dimensional reference temperature.

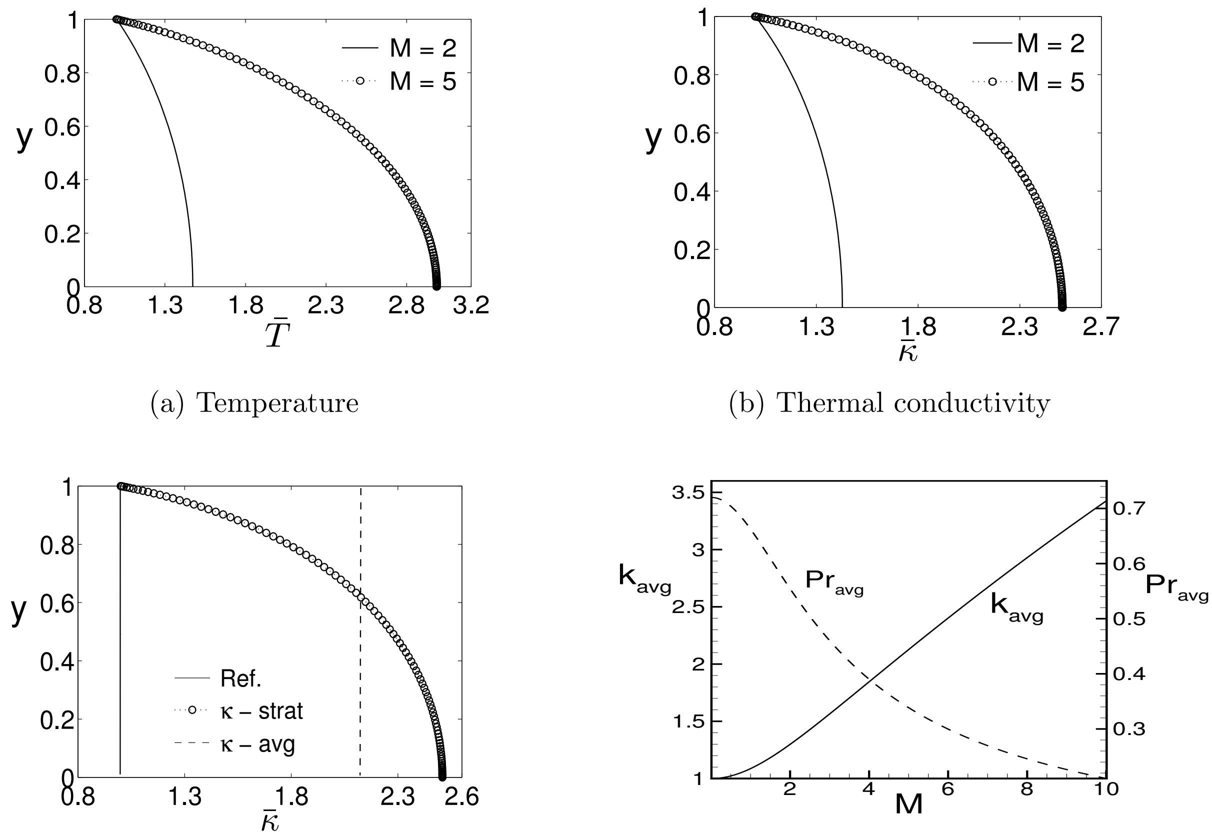

(a) Temperature

(b) Thermal conductivity

(c) Thermal conductivity

(d) Average conductivity and Prandtl number

FIG. 2: The variation of (a) mean temperature and (b) mean conductivity along the wall-normal direction for a κ-stratified flow at two Mach numbers; (c) comparison of conductivity variation in the three base flows defined in section II A at $M = 5$; (d) average thermal conductivity and Prandtl number for a range of Mach numbers. Reference Prandtl number considered is 0.72.

$$\bar{\kappa} = \bar{T}^{3/2}\frac{(1+B)}{(\bar{T}+B)}, \text{where } B = \frac{194\text{ K}}{T_{ref}}. \tag{3}$$

Since the lower wall is adiabatic, using Eq. 3, the energy equation (Eq. 2) can be reduced to

$$\frac{d\bar{T}}{dy} = -\left(\gamma-1\right)M^2 Pr\,\frac{\left(\bar{T}+B\right)}{\bar{T}^{3/2}\left(1+B\right)}\,y. \tag{4}$$

With an initial guess for temperature at the lower wall, the above equation is solved numerically using 4^{th} order Runge Kutta method, till the upper wall temperature reaches its reference value (= 1).

The base flow thus obtained is presented in Fig. 2, for a Prandtl number of 0.72 and a reference temperature of 220.8 K. Figure 2a compares the variation in temperature along the wall-normal direction at two Mach numbers 2 and 5. Starting from the same reference quantities at the top wall, temperature increases and attains a maximum value at the bottom adiabatic wall. The gradient in temperature thus increases with the flow Mach number. As expected, the thermal conductivity exhibits similar variation with wall-normal distance and Mach number (see Fig. 2b). The mean conductivity $\bar{\kappa}$ is higher at every point in the κ-stratified flow as compared to the reference flow with constant values of viscosity and thermal conductivity. Therefore, the κ-stratified flow can be viewed as a superposition of an increase in the average value of thermal conductivity, and an imposed conductivity variation across the shear layer. The average value of conductivity is defined as,

$$\bar{\kappa}_{avg} = \int_0^1 \bar{\kappa} dy. \tag{5}$$

We construct another model problem with this average value of conductivity and the reference value of viscosity, both constant across the shear layer, and refer to it as the κ-averaged flow. Figure 2c compares the κ-stratified flow at Mach 5 to the corresponding reference and the κ-averaged flows.

The effect of the gradients in conductivity on flow stability can be obtained by comparing the κ-averaged flow with the κ-stratified case. On the other hand, a comparison of the reference flow with the κ-averaged case will bring out the effect of enhanced conductivity. This can be considered as comparing two uniform viscosity, but different Prandtl number flows, resulting from two different values of conductivities. The Prandtl number in the case of the κ-averaged flow is much lower than that of the reference flow, and is defined as $Pr_{avg} = Pr/\bar{\kappa}_{avg}$. Figure 2d shows that the κ_{avg} sharply increases, whereas Pr_{avg} decreases with Mach number.

B. μ-stratified flow

In the case of μ-stratified flow, conductivity is kept constant ($\bar{\kappa} = 1$) at its reference value, and viscosity is varied as a function of temperature using Sutherland's formula (Eq. 7). With a constant value of the shear stress ($= \tau$) at the wall, the momentum equation in the streamwise direction can be written as,

$$\bar{\mu} \frac{d\bar{U}}{dy} = \tau \text{ (constant)}, \tag{6}$$

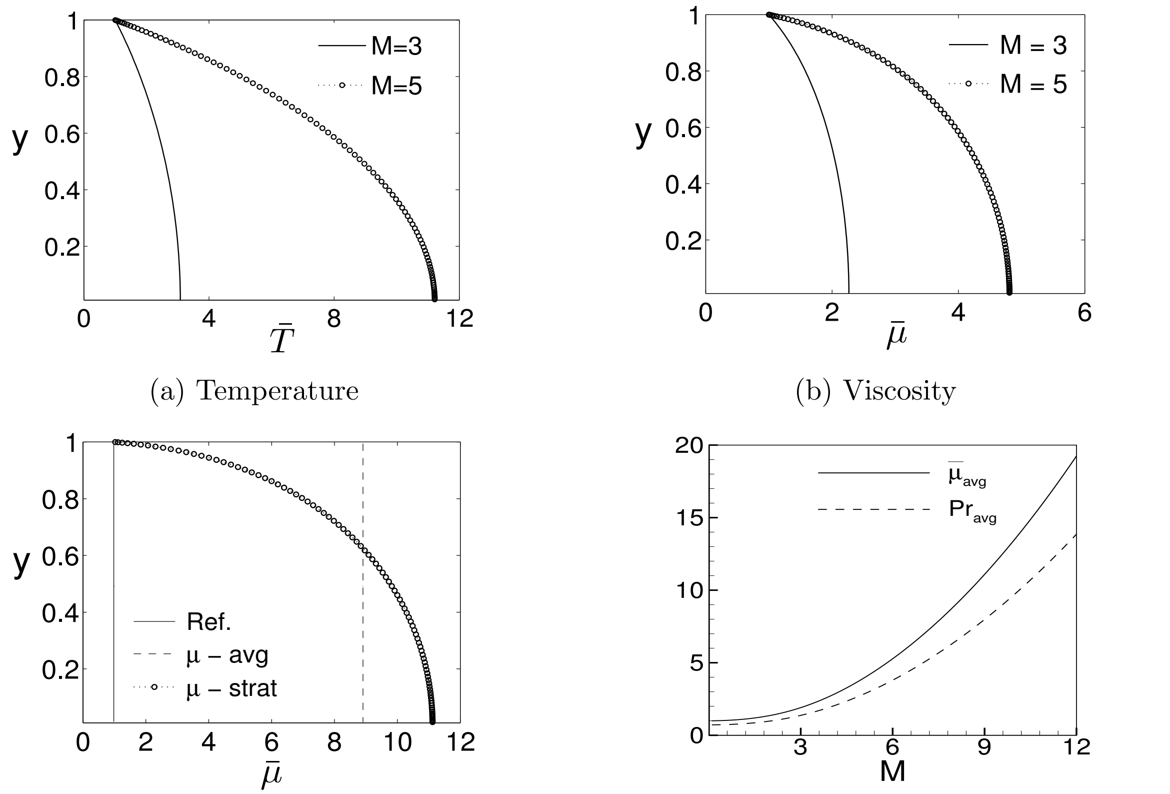

(a) Temperature

(b) Viscosity

(c) Viscosity for three model problems

(d) Average viscosity and Prandtl number

FIG. 3: The variation of (a) mean temperature and (b) mean viscosity along the wall-normal direction for a μ-stratified flow at two Mach numbers; (c) comparison of viscosity variation in the three base flows defined in section II B at $M = 5$; (d) average viscosity and Prandtl number for a range of Mach numbers. Reference $Pr = 0.72$.

$$\text{where} \quad \bar{\mu} = \bar{T}^{\frac{3}{2}} \frac{(1+C)}{\left(\bar{T}+C\right)}, \text{ and } C = \frac{110.4 \text{ K}}{T_{ref}}. \tag{7}$$

For a lower adiabatic wall, using Eq. 6, the energy equation (Eq. 2) can be integrated such that $\bar{U}$ becomes 1 when $\bar{T} = 1$. This leads to the following equation for temperature as a function of base flow velocity:

$$\frac{\bar{T} - C}{\sqrt{\bar{T}}} = \frac{(\gamma - 1)\, M^2 Pr}{4} \left(1 - \bar{U}^2\right)(1 + C) + (1 - C), \tag{8}$$

which can be expressed completely in terms of $\bar{U}$ such that the shear stress can be found iteratively using the shooting method. Eq. 9 can be numerically integrated for $\bar{U}$ with the initial condition $\bar{U}(0) = 0$, and finding the value of τ for which $\bar{U}(1) = 1$.

$$\frac{d\bar{U}}{dy} = \frac{\tau}{\bar{\mu}(\bar{T})} = \frac{\tau}{\mu(\bar{U})} = f(\bar{U}), \tag{9}$$

The base flow obtained for a reference Prandtl number and temperature of 0.72 and 220.8 K respectively, is presented in Fig. 3. The variation of temperature and viscosity in this case are qualitatively the same to those presented in Fig. 2. The temperature levels are, however, much higher in the μ-stratified flow than those in the corresponding κ-stratified cases, due to higher viscous dissipation. The viscosity profiles in the μ-stratified flows can be interpreted as an increase in the average value of viscosity across the entire shear layer plus a viscosity gradient imposed across the flow. Similar to the conductivity cases described in section II A, we can define an average fluid viscosity as

$$\bar{\mu}_{avg} = \int_0^1 \bar{\mu} dy, \tag{10}$$

and use it to define a μ-averaged model Couette flow, which has a constant viscosity ($\bar{\mu}_{avg}$) and the reference value of conductivity across the shear layer. The viscosity variation in the reference flow, the μ-averaged flow and the μ-stratified flows are shown in Fig. 3c for a Mach number of 5. The effect of viscosity stratification is determined by comparing the μ-averaged flow with the μ-stratified flow, since both have the same average value of mean fluid viscosity ($\bar{\mu}$). The average fluid viscosity ($\bar{\mu}_{avg}$) and the corresponding average Prandtl number ($Pr_{avg} = \bar{\mu}_{avg}\, Pr$) are plotted as a function of Mach number in Fig. 3d for a reference Prandtl number of 0.72. It can be observed that the average value of viscosity increases rapidly with Mach number, which leads to a sharp increase in the Pr_{avg} value.

C. μ-κ-stratified flow

In the case of a μ-κ-stratified flow, thermal conductivity and viscosity vary independently with temperature, as per Eqs. 3 and 7, respectively. From Eqs. 1 and 2, we obtain

$$\frac{d^2\bar{T}}{dy^2} + \frac{1}{\bar{\kappa}}\frac{d\bar{\kappa}}{d\bar{T}}(\frac{d\bar{T}}{dy})^2 + \frac{(\gamma-1)\, M^2 Pr\, \tau^2}{\bar{\mu}\, \bar{\kappa}} = 0, \tag{11}$$

which is solved using the 4^{th} order Runge Kutta method, where the shear stress τ and the lower wall temperature are found iteratively such that $\bar{U}(1) = 1$ and $\bar{T}(1) = 1$. Fig. 4 presents the base flow velocity and temperature profiles for a μ-κ-stratified flow at $M = 2$

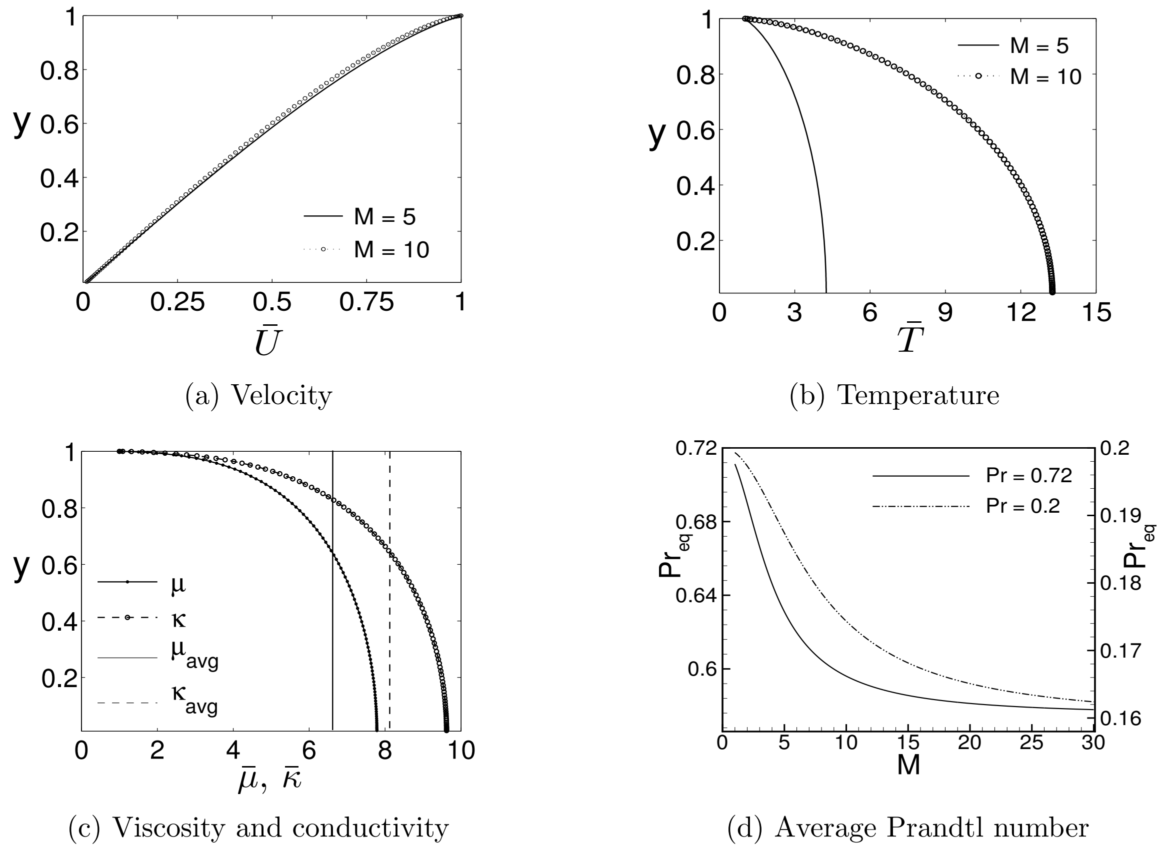

(a) Velocity

(b) Temperature

(c) Viscosity and conductivity

(d) Average Prandtl number

FIG. 4: The variation of (a) mean velocity and (b) mean temperature along the wall-normal direction for a μ-κ-stratified flow at two Mach numbers; (c) comparison of viscosity and conductivity variation in the three base flows defined in section II C at $M = 5$; (d) comparison of average Prandtl number for a range of Mach numbers at reference Prandtl number of 0.72 and 0.2.

and 5. The reference temperature and Prandtl number considered are same as earlier. Comparing Fig. 4b with Figs. 2a and 3a, we can infer that temperature in a μ-κ-stratified flow is intermediate between the μ-stratified and κ-stratified flows, with the same reference values of Mach and Prandtl numbers.

To determine the effect of simultaneous gradients in viscosity and conductivity, an average flow is constructed with constant values of $\bar{\mu}$ and $\bar{\kappa}$, obtained from the equivalent μ-κ-stratified flow, by taking the average of viscosity and conductivity (using Eqs. 5 and 10). The effect of increase in the magnitude of both $\bar{\mu}$ and $\bar{\kappa}$ on flow stability can be realized by comparing the μ-κ-averaged flow with the reference flow, having $\bar{\mu}$ and $\bar{\kappa}$ equal to 1. The variations in viscosity and conductivity along the wall-normal direction are shown for a μ-κ-stratified flow, at $M = 5$ and $Pr = 0.72$, along with their corresponding average values in Fig. 4c. It can be noted that for the current transport model considered, thermal conductivity has a larger variation with temperature compared to viscosity, which results in a lower value of the average Prandtl number ($Pr_{avg} = Pr\ \bar{\mu}_{avg}/\bar{\kappa}_{avg}$) at higher Mach numbers (see Fig. 4d).

We note that stratification of transport properties alters the mean flow profiles for a fixed Mach and Reynolds number. There are large changes in the mean temperature profile, especially at high Mach numbers, which alters the stability characteristics of the flow significantly. In addition, the gradients in viscosity and conductivity appear in the perturbation equations (presented in section III.A and appendix 1), and thus influence the dynamics of the disturbances. The present study does not attempt to isolate the effects of viscosity and conductivity on the perturbation alone from those which act on the perturbations through changes in the mean flow. It is possible that the majority of the effects presented here are a result of base flow variations due to the changes in transport property across the flow. In fact, the results presented in the paper are a combination of both the effects, as will be expected in any real flow with transport property variations.

III. DETAILS OF STABILITY ANALYSIS

A. Linear stability theory

Instantaneous flow quantities (A), such as velocity, density or temperature, are expressed as a sum of the mean flow variable ($\bar{A}$) and a small fluctuation quantity ($\tilde{A}$), i.e.,

$$A = \bar{A}\,(y) + \tilde{A}\,(x, y, z, t)\,. \tag{12}$$

The linearized equations for the disturbances are obtained by substituting Eq. 12 into the non-dimensional form of the governing equation and neglecting the non-linear and higher order terms in the fluctuations. We assume a normal mode form for the fluctuations as,

$$\tilde{A}\,(x, y, z, t) = \hat{A}\,(y)\ e^{\,i\,(\alpha\, x + \beta\, z - \omega\, t)}, \tag{13}$$

where $\hat{A}$, α, β and ω represent disturbance amplitude, streamwise and spanwise wavenumbers and frequency respectively. A temporal stability analysis is carried out in this work, which requires ω to be complex and α, β both are real parameters. Substituting Eq. 12 into the disturbance equations, we obtain a homogeneous system of ordinary differential equations, which can be expressed as,

$$B\psi = \omega\, I\, \psi. \tag{14}$$

where $\psi = (\hat{u},\ \hat{v},\ \hat{w},\ \hat{\rho},\ \hat{T})^{\,tr}$ represents the vector of the complex amplitudes of the flow variables, and I is the identity matrix. The elements of matrix B are mentioned in the appendix 1, and they are functions of α, β, ω, Re, Pr, M and the mean-flow variables.

The velocity fluctuations satisfy the no-slip boundary condition at both the walls. Isothermal and adiabatic boundary conditions are applied on the temperature fluctuations at the upper and the lower walls respectively. The momentum equation in the wall-normal direction is solved to obtain the boundary condition for density. With the help of these boundary conditions, and with discretization by the Chebyshev spectral collocation method, the eigenvalue problem is solved using the QZ algorithm of MATLAB. This provides the complex frequency $\omega = \omega_r + i\,\omega_i$, where ω_i represents the growth or decay rate of the disturbance. We have used 150 Chebyshev points to compute the eigenvalues, and the results presented in this paper are grid converged. The validation of the numerical method is presented in appendix 3.

The eigenspectrum for a plane compressible Couette flow consists of a Y-shaped viscous branch. The acoustic modes form a dome-like structure above the viscous modes (see Ref. [30]). The stability characteristics of a Couette flow is determined by the acoustic modes. Physically, these modes appear due to sustained reflection of acoustic waves between the wall and a relative sonic line. Refs. [20], [21] and [22] provide a detailed description of classifying the acoustic modes. In the limit of $\alpha \to 0$, the odd acoustic modes (1, 3,...) are the ones with phase speed greater than unity, whereas the even (2, 4, ...) acoustic modes have phase speed less than zero. The odd modes show acoustic wave reflection at the lower wall, and the even modes have sound wave reflection at the top wall. Pressure patterns corresponding to the first few acoustic modes are shown in Refs. [20] and [30].

We note that the linear stability results presented in the paper are for $\beta = 0$. This is based on the finding that two-dimensional disturbances are the least stable modes for compressible Couette flows, as reported by Malik et al. [22] for systematically varying β values (see Fig. 7 in Ref. [22]).

B. Transient growth analysis

Non-modal analysis or transient growth is used to study the short-term dynamics of a system. The parameter space where the flow is predicted to be linearly stable is the region of interest for transient growth. It investigates the possibility of transient non-modal amplification of initial disturbance energy, in a flow that supports only decaying eigenvalues and is thus nominally stable. Cases where such transient amplification can trigger nonlinearities, and even cause a linearly stable flow to undergo transition to turbulence are now well known, e.g., incompressible Couette flow. In a compressible medium, velocity field is coupled with temperature, therefore, the changes in temperature and density have to be considered. A suitable norm for a compressible flow is the one which accounts for internal energy changes in addition to the disturbance kinetic energy. The norm has to be such that it can eliminate energy transfer associated with pressure, since the compression work is conservative [25]. Therefore, for evaluating the temporal energy growth, we have used the Mack's energy norm, which is

$$2E = \int_0^1 \bar{\rho}\left(|u_s|^2 + |v_s|^2 + |w_s|^2\right) + \frac{\bar{T}}{\gamma\bar{\rho}M^2}|\rho_s|^2 + \frac{\bar{\rho}}{\gamma(\gamma-1)\bar{T}M^2}|T_s|^2\, dy, \tag{15}$$

here the subscript s is used to denote the state vector ($\phi = [u_s,\, v_s,\, w_s,\, \rho_s,\, T_s]^{tr}$), which can be expressed in terms of the eigenvectors (ψ) and the expansion coefficients (χ) as,

$$\phi = \sum_{k=1}^{n} \chi_k(0)\exp(-i\omega_k t)\psi_k, \tag{16}$$

and n is the number of eigenvalues used to compute the transient energy growth. In terms of eigenvector expansion, we can write Eq. 15 as,

$$2E = (\mathit{\Lambda}\,\chi)^H \left[\int_0^1 Q^H\, \mathbf{M}\, Q\, dy\right] \mathit{\Lambda}\,\chi. \tag{17}$$

Here, H denotes the Hermitian matrix, and $\mathit{\Lambda}$ is a diagonal matrix with elements $e^{-i\,\omega\,t}$. The columns of matrix Q contains the eigenvectors in the truncated vector space, and the matrix $\mathbf{M}$ includes the coefficients of the disturbances in Eq. 15. Due to its positive definite nature, we can write the integral in Eq. 17 as a product of matrix F and its Hermitian F^H. Using the eigenvector basis, the matrix F can be calculated using the Cholesky decomposition. The energy norm can be simplified in terms of matrix F and the eigenvector expansion coefficients as,

$$2E = ||F\Lambda\chi||^2. \tag{18}$$

Now, the optimal transient growth of disturbance energy is given by,

$$G = max\,\frac{E(t)}{E(0)} = max\,\frac{||F\Lambda\chi||^2}{||F\chi||^2} = ||F\Lambda F^{-1}||^2, \tag{19}$$

which is determined by the singular value decomposition. The right singular vector corresponding to the largest singular value provides the expansion coefficients of the optimal perturbation. For a certain combinations of streamwise and spanwise wavenumbers, we can obtain the maximum energy amplification at a given time $G(\alpha, \beta, t)$. The perturbation energy can also be optimized over all time $G_{max}(\alpha, \beta)$. More detailed discussions on transient growth can be found in Refs. [25], [26], [27] and [28]. We have used the eigenvalues with decay rate greater than 0.5 ($\omega_i > -0.5$) to compute the transient energy amplification for all the cases presented in this paper.

The choice of norm can make significant difference to the transient growth results. Our calculation show that using a kinetic energy norm, without the contributions of thermodynamics perturbations, can predict much higher energy amplification compared to that obtained using the Mack norm. The results are similar to those presented by Tempelmann et al. [31] for compressible boundary layer flows with low wall temperatures, and highlight the importance of including thermodynamic perturbations for the calculation of the total energy of the disturbances.

IV. STABILITY RESULTS

A. Conductivity stratification

Linear stability results in the Mach number-wavenumber plane

Figure 5 plots the growth rate contours for the least stable mode for varying Mach number and disturbance wave number. A large range of Mach number up to 20 is considered, and the results are representative of high Mach number perfect gas flow. The Reynolds number and reference Prandtl number considered are 10^5 and 0.72 respectively. The regions within the loops are unstable, bounded by the neutral growth rate contours. The stability characteristics of the reference flow with $\bar{\mu} = 1$ and $\bar{\kappa} = 1$ is shown in Fig. 5a. The corresponding conductivity-stratified flow is presented in Fig. 5d, where viscosity is maintained at its reference value, such that Reynolds number is 10^5 for the entire range of Mach numbers. Figure 5c shows the results for the κ-averaged flows, with uniform conductivity maintained at the $\bar{\kappa}_{avg}$ value, computed for each Mach number. Comparison of Fig. 5c and 5d thus bring out the isolated effect of conductivity stratification at each Mach number. This is in contrast to earlier works (for example, Ref. [22]), which report the combined effect of the variation in the magnitude and gradient of transport properties on Couette flow stability.

Noting that the value of $\bar{\kappa}_{avg}$ is a strong function of Mach number (see Fig. 2d), we present the stability characteristics of Couette flows with varying Mach number, but $\bar{\kappa}_{avg} = 3.3$ for all, in Fig. 5b. This value of $\bar{\kappa}_{avg}$ is obtained by averaging over the entire range of Mach number ($0.1 \leq M \leq 20$). Figure 5b thus separates the effect of varying Mach number, keeping the thermal conductivity constant at an elevated level as compared to the reference flow, whereas Fig. 5c has the combined effect of both $\bar{\kappa}_{avg}$ and M varying simultaneously.

It can be observed that enhancement in the thermal conductivity in Fig. 5b and 5c increases the number of instability loops compared to the reference flow in Fig. 5a. This implies that a larger Mach number range of flows are linearly unstable at higher conductivity, and at each Mach number, the unstable disturbances span a wider range of spatial wave numbers. The maximum growth rates observed in Fig. 5b and 5c are in the range of $\omega_i \simeq 0.05$, which is higher than those in the reference flow ($\omega_i = 0.004$) by an order in magnitude. Thus, a faster rate of heat diffusion compared to momentum has a strong destabilizing effect on compressible Couette flow, all other factors kept constant.

By comparison, the effect of conductivity stratification is much less prominent. The least stable mode in the κ-stratified flow (Fig. 5d) has comparable growth rate as the corresponding κ-averaged flow in Fig. 5c. There are, however, additional instability loops (top right corner of the plot) in the the κ-stratified flow at high Mach numbers ($10 < M < 20$) representing unstable regions, spanning over a wide range of streamwise wavenumbers.

In the context of incompressible flows, Sameen and Govindarajan [17] study the effect of heat diffusivity on the stability of a channel flow of liquid, with both symmetric and asymmetric heating. They find that the least stable mode is practically unaffected by a change in the heat diffusivity or Prandtl number, as per linear stability theory. This is in contrast to the current stability results in compressible Couette flow, where we notice a strong destabilizing effect of increase in the magnitude of thermal conductivity. Sorokin [10]

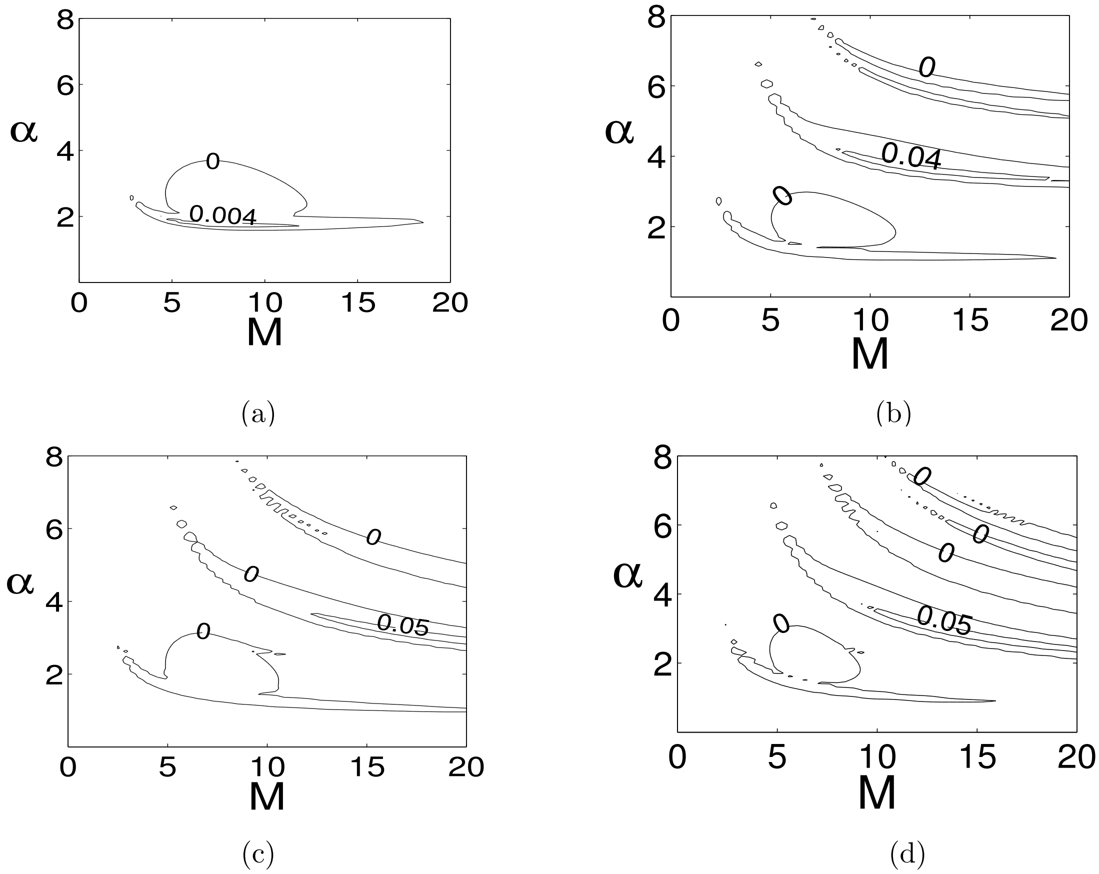

FIG. 5: Comparison of stability diagrams in the Mach-streamwise wavenumber plane for (a) the reference flow, (b) κ-averaged flow, with $\bar{\kappa}_{avg} = 3.33$; (c) κ-averaged flow with $\bar{\kappa}_{avg}$ varying with Mach number; and (d) κ-stratified flow. Here, reference Prandtl number and Reynolds number are 0.72 and $Re = 10^5$, respectively and $\beta = 0$.

reports a similar destabilizing role of thermal conductivity, for a fluid layer over a vertical plane, where relatively small changes in the thermal conductivity can destabilize the flow.

Stability analysis in Reynolds number-wavenumber plane

Figure 6 plots the least stable growth rates in the Reynolds number-streamwise wavenumber plane for a two-dimensional disturbance at Mach 10. The stability diagrams for the reference and the κ-stratified flows are presented in Figs. 6a and 6c respectively, for a reference Prandtl number of 0.72. Figure 6b represents the κ-averaged flow, with an average Prandtl number of 0.21, corresponding to the κ-stratified flow shown in Fig. 6c. Once again, the differences observed in the stability characteristics between the reference flow (Fig. 6a) and the κ-averaged flow (Fig. 6b) are solely due to an increase in the magnitude of thermal conductivity,

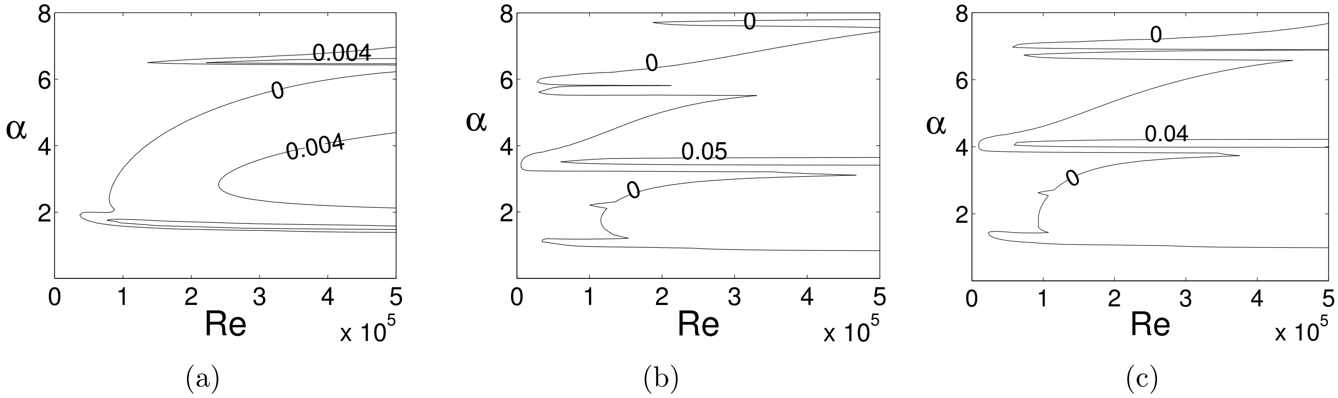

FIG. 6: Comparison of growth rate contours in the Re-α plane for (a) the reference flow, (b) κ-averaged flow with $Pr_{avg} = 0.21$, and (c) κ-stratified flow. Reference Prandtl number and Mach number considered are 0.72 and 10 respectively.

with no gradient in $\bar{\kappa}$ across the flow.

An increase in the magnitude of $\bar{\kappa}$, leading to a decrease in the Prandtl number (from 0.72 to 0.21), increases the maximum disturbance growth rate by about 10 times – from 0.004 in the reference flow to 0.05 in the κ-averaged flow. The number of instability loops and the area covered by them in the Re-α plane also increase significantly for flows with higher thermal conductivity.

Table I lists the critical Reynolds numbers (Re_{cr}) for the reference, κ-averaged and κ-stratified Couette flows, at different Mach numbers. Two different reference Prandtl numbers (0.72 and 0.2) are considered, and the Pr_{avg} values in the corresponding κ-averaged flows are also tabulated. A large change in the critical Reynolds number is observed due to an increase in the mean thermal conductivity from its reference value of 1 to κ_{avg}. For $M = 10$ and reference $Pr = 0.72$, Re_{cr} decreases from 36437 to 5537. The wavenumber (α_{cr}) corresponding to the critical Reynolds number increases from 1.93 to 3.41, implying a change in the instability loop that contributes to Re_{cr}, from the first to the second loop (in Fig. 6a and 6b). This is often associated with a change in the dominant instability, from first to the second acoustic mode, as detailed in Ref. [30].

The effect of stratification in conductivity can be realized by comparing Figs. 6b and 6c, which are two flows with the same average value of conductivity, and the difference being the stratification in $\bar{\kappa}$. The κ-averaged flow has slightly higher maximum growth rate (0.05 in Fig. 6b as compared to 0.04 in Fig. 6c), in addition to an increase in number of instability loops. However, the most unstable mode comes from the second loop in both the cases.

TABLE I: Comparison of critical Reynolds number and wavenumber at various Mach numbers for three base flows with different conductivities and uniform viscosity. Reference Prandtl numbers considered are 0.72 and 0.2.

		Re_{cr}				α_{cr}		
Pr	M	Reference	κ-avg	κ-strat	Pr_{avg}	Reference	κ-avg	κ-strat
0.72	3	40555	28051	27426	0.46	2.58	2.41	2.52
0.72	5	19527	13290	12252	0.34	2.18	1.79	1.97
0.72	8	27210	6136	10434	0.25	1.98	4.01	4.63
0.72	10	36437	5537	8860	0.21	1.93	3.41	4.03
0.2	3	9704	8311	9241	0.17	2.43	2.41	2.40
0.2	5	10442	6659	7665	0.14	5.22	4.76	4.92
0.2	8	4672	2715	3530	0.10	3.71	3.03	3.27
0.2	10	5232	2474	3831	0.09	3.34	2.51	2.79

Table I shows that, the critical Reynolds number for both the cases are relatively close compared to the reference flow.

Whether conductivity stratification has any significant effect depends on the Mach number and the reference Prandtl number. For example, in the case of $Pr = 0.72$, the κ-averaged flow behaves similar to the κ-stratified flow at $M = 3$ and 5, with a marginal stabilization, whereas at higher Mach numbers (8 and 10, see Table I), the κ-averaged flow is significantly more unstable. On the other hand, for a low reference Prandtl number of 0.2, a stratification in thermal conductivity stabilizes the flow at all Mach numbers. In these cases, κ-averaged flow is the least stable amongst all the three flows.

Transient growth results

Figure 7 presents the maximum temporal energy amplification (G_{max}) as a function of streamwise and spanwise wavenumbers. To investigate the effect of conductivity stratification on the transient energy growth, we compare the κ-stratified flow (Figs. 7c and 7f) with the κ-averaged (Figs. 7b and 7e), and the reference flow (Figs. 7a and 7d). The first three

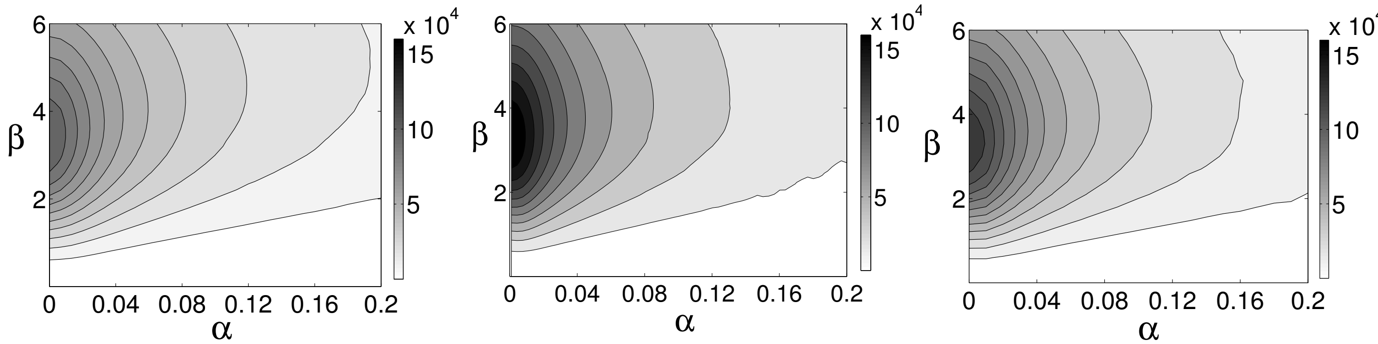

(a) Reference flow (b) κ-averaged (c) κ-stratified

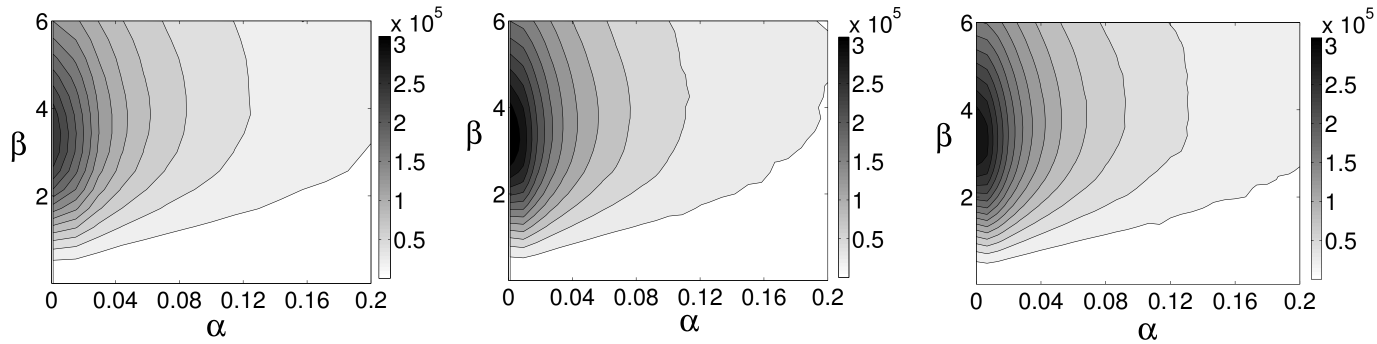

(d) Reference flow (e) κ-averaged (f) κ-stratified

FIG. 7: Contours of maximum temporal energy amplification G_{max} in the wavenumber plane, showing the effect of increase in the magnitude of conductivity and its stratification at $M = 5$. The reference Pr for (a) and (c) is 0.7, while (d) and (f) are at $Pr = 0.2$. Prandtl number corresponding to the averaged flows (b) and (e) are 0.33 and 0.14 respectively.

sets of plots are at a reference $Pr = 0.7$, while the remaining figures are presented at a lower reference Prandtl number of 0.2.

We note that an elevated thermal conductivity in the κ-averaged flow leads to a large effect on the transient energy growth, compared to the stratification in mean conductivity. The maximum energy amplification increases significantly from the reference to the κ-averaged flow, with minimal changes between the κ-averaged and κ-stratified flows. This trend is valid at both Prandtl numbers, although reducing the reference Prandtl number from 0.7 to 0.2 leads to a higher amplification of energy irrespective of the type of flow considered. The data in Fig. 7 corresponds to Mach 5. Similar effects of magnitude and gradient in mean conductivity on transient energy amplification is observed at higher Mach numbers, but the energy amplification decreases significantly with increase in the Mach number [26].

For Mach 5 and Prandtl number of 0.2, the Re_{cr} for the κ-averaged flow is lower than the

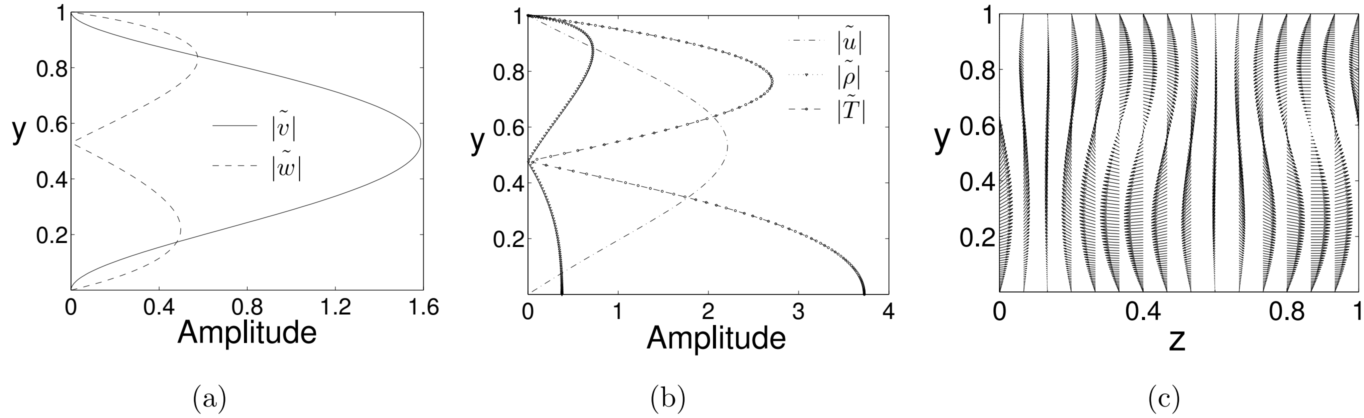

FIG. 8: Optimal disturbance for a κ-stratified Couette flow at $M = 10$, $Re = 10^5$, $\alpha = 0$, $\beta = 3.36$, and reference $Pr = 0.2$. Figures (a) and (b) show the amplitude of the optimal disturbance before and after amplification, respectively. The flow pattern of the optimal disturbance in $y - z$ plane at $t = t_{opt}$ is presented in Fig. (c).

κ-stratified flow (see Table I). The transient growth data also follows the same trend, with the κ-averaged flow having the highest energy amplification (Fig. 7e). The trend observed in the transient growth data at the higher Prandtl number ($= 0.7$) is however opposite to the linear stability results, namely, the κ-stratified flow is the most modally unstable at Mach 5 and $Pr = 0.7$. For incompressible flows, Sameen and Govindarajan [17] observe a large destabilizing effect of increasing the Prandtl number or reducing the heat diffusivity on the transient growth of disturbance kinetic energy for a channel flow, though linear stability predicts negligible effect of varying heat diffusivity.

We note that the current work uses the temporal framework, for both modal and non-modal stability. Other works studying transient growth in compressible flows employ the spatial framework, because of its relevance to practical applications. For modal analysis, Gaster's transformation can be used for small growth rates. However, to the best of our knowledge, no theoretical framework exists to formally relate spatial and temporal gain factors for non-modal growth. Direct comparison between spatial and temporal energy amplification for incompressible boundary layers is presented in Ref. [29]. They report a good match between scaled temporal gain factors with the corresponding spatial results, and that the scaling factors for the energy amplification are of order one. In a recent work on high-speed boundary layers, Bitter and Shepherd [26] show a qualitative match (with small differences) between temporal and spatial gain factors computed at identical Mach and Reynolds numbers. Thus, the temporal amplification rate reported in the current work, may be taken as a good indicator of the expected transient growth in a spatial transient growth analysis. Specifically, the dominant effects of transport property on the energy gain factor may be extrapolated to the spatial framework as well. This includes the large destabilizing role of enhanced conductivity between the reference and κ-averaged flows, and a relatively small effect of conductivity stratification, as shown in Fig. 7. The effects of viscosity stratification (section IV.B) and a combined viscosity-conductivity stratification (section IV.C) may be interpreted in the context of spatial analysis in a similar way.

Figure 7 shows that maximum amplification of the transient energy occurs for a streamwise independent disturbance ($\alpha = 0$). This is valid for all the three base flow cases considered in Fig. 7, with any Prandtl and Mach number. The shape of the optimal disturbance for a κ-stratified flow at $M = 10$, $Re = 10^5$ and $Pr = 0.2$ is presented in Fig. 8. The spanwise wavenumber of 3.36 considered here corresponds to the maximum transient energy gain. The absolute values of the disturbances are plotted along the wall-normal direction in Figs. 8a and 8b. We notice that the optimal disturbance before amplification consists of mainly spanwise and normal components of velocity, other fluctuations are negligibly small. After amplification, the disturbance is mostly composed of streamwise velocity, temperature and density fluctuations, other fluctuations are relatively small in magnitude (see Fig. 8b). The velocity vectors plotted in the $y-z$ plane corresponding to the amplified optimal disturbance shows the formation of two counter rotating streamwise independent vortices, which lift the low-momentum and high temperature flow up from the adiabatic bottom wall and push down the high-momentum, low temperature flow causing the formation of streaks in velocity and temperature. This is the well-known lift-up mechanism which leads to the transient energy growth.

By analyzing both the linear stability and transient growth results, we conclude that, a κ-stratified flow behaves closely similar to the κ-averaged flow, with the same average value of conductivity, and reference viscosity. Also, these two base flows are far more unstable, compared to the reference flow for all Mach and reference Prandtl numbers. In other words, the main effect of stratification is captured by the net increase in thermal conductivity.

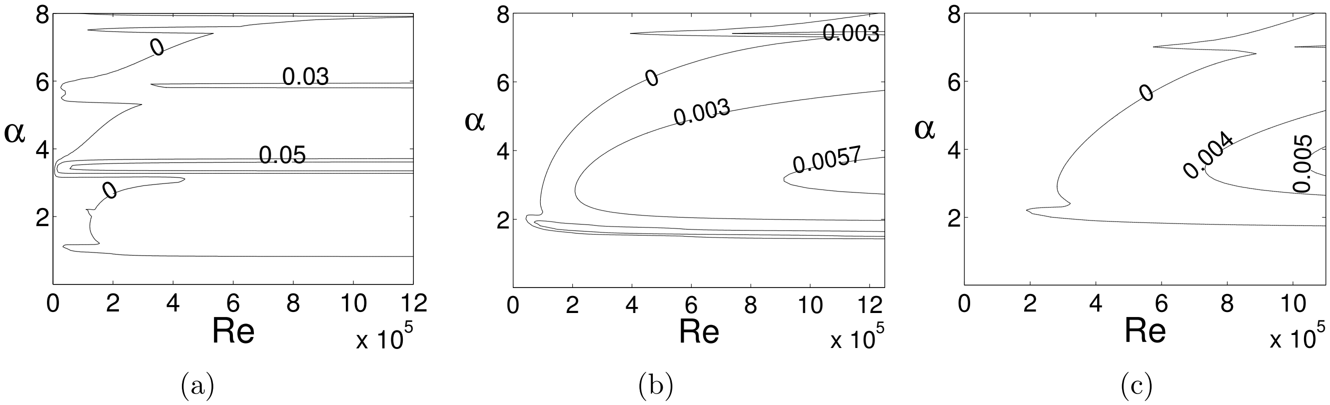

FIG. 9: Comparison of growth rate contours in the Re-α plane for (a) the reference flow, (b) μ-averaged flow with $Pr_{avg} = 0.85$, and (c) μ-stratified flow. Reference Prandtl number and Mach number considered are 0.2 and 10 respectively.

B. Viscosity stratification

Linear stability results in the Reynolds number-wavenumber plane

Figure 9 shows the growth rate contours in the Reynolds number and the streamwise wavenumber plane for a Couette flow, at $M = 10$ and reference $Pr = 0.2$. The stability diagrams for the reference and the stratified viscosity flow are plotted in Figs. 9a and 9c respectively. The average mean viscosity corresponding the μ-stratified flow at $M = 10$ and $Pr = 0.2$, is taken as the mean viscosity for the μ-averaged flow, presented in Fig. 9b.

We notice that for a given Reynolds number, the reference flow is the least stable ($\omega_i \simeq 0.05$ in Fig. 9a), with an order of magnitude higher maximum growth rate compared to the other two base flow cases ($\omega_i \simeq 0.005$ in Figs. 9b and 9c). It also has a larger region of instability in the Re-α plane. The enhancement in the mean viscosity value from 1 to 4.2 and a consequent increase in the Prandtl number (from 0.2 in the reference flow to 0.85 in the μ-averaged flow) makes the μ-averaged flow more stable compared to the reference flow. The reduction in the Reynolds number, caused by an increase in the viscosity value, also contributes to the low growth rates observed in the μ-averaged flow.

The effect of stratification in viscosity is realized by comparing Fig. 9b with 9c. Both the μ-averaged and μ-stratified flows have similar maximum growth rates, however the stratification in viscosity shifts the instabilities to a higher Reynolds number.

The strong stabilizing effect of viscosity gradient can also be noticed from Table II, which lists the critical Reynolds numbers, and the corresponding disturbance wave numbers, for

TABLE II: Critical Reynolds number (Re_{cr}) and wavenumber (α_{cr}) at various Mach numbers for three different base flows with uniform conductivity, and different values of viscosities. Reference Prandtl numbers considered are 0.5 and 0.2.

		Re_{cr}				α_{cr}		
Pr	M	Reference	μ-avg	μ-strat	Pr_{avg}	Reference	μ-avg	μ-strat
0.5	3	29488	46014	147874	0.8	2.44	2.63	2.77
0.5	5	15136	53397	283789	1.46	1.98	2.63	2.79
0.5	7	18860	233130	2416502	2.52	1.79	3.00	3.17
0.2	3	9704	12148	20784	0.24	2.43	2.45	2.26
0.2	5	10442	13267	25484	0.34	5.22	1.79	1.92
0.2	10	5232	41876	187900	0.85	3.34	2.05	2.21

different values of Mach and reference Prandtl numbers. For example, at $M = 5$ and reference $Pr = 0.5$, the critical Reynolds number for the μ-stratified flow is 283789, which is around five times larger than the corresponding μ-averaged flow. The same trend is also observed at other Mach and Prandtl numbers, with a stronger stabilizing effect of viscosity gradient at higher Mach numbers. Increasing the reference Prandtl number from 0.2 to 0.5, also increases Re_{cr} (see Table II) for all the flow cases considered, and thus leads to a more stable flow at higher Pr. A similar stabilizing effect of viscosity stratification is also reported in Ref. [22] for a compressible Couette flow. However, the work includes the variation of viscosity and conductivity simultaneously, since a constant Prandtl number is used in their formulation.

In contrast to our compressible results, where we observe a strong stabilizing role of increase in the magnitude of viscosity, the linear stability results for incompressible flows predicts that, decreasing the viscosity towards the wall is stabilizing. Also, if there exists any temperature difference in the flow, the critical Reynolds number increases for low-speed flows. Amongst various studies, this is recently shown in Ref. [17], for a channel flow of liquids, maintained between two walls of different temperatures.

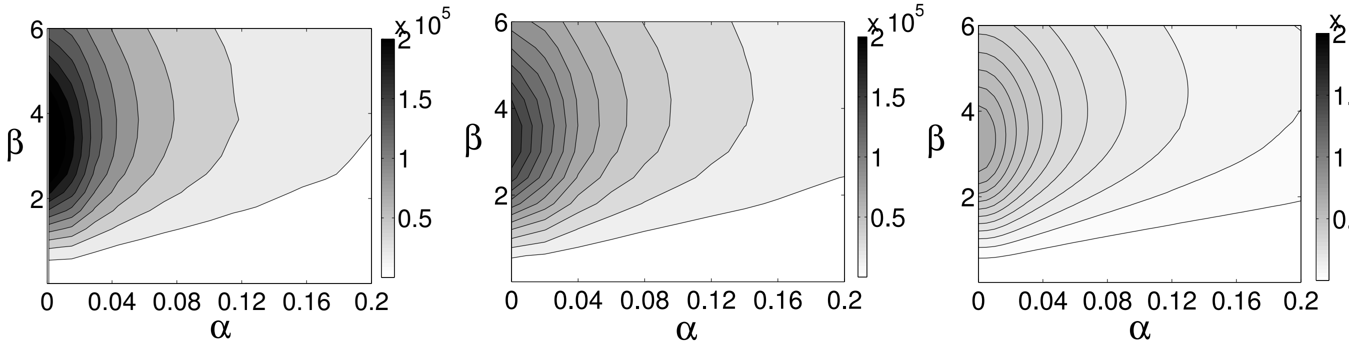

(a) (b) $Pr_{avg} = 0.34$ (c)

FIG. 10: Contours of maximum temporal energy amplification G_{max} in the wavenumber plane, showing the effect of stratification in viscosity. Figures (*a*), (*b*) and (*c*) represent the reference, μ-averaged and μ-stratified flows, respectively at $M = 5$ and $Re = 10^5$. The reference Prandtl number is 0.2.

Transient growth results

To study the effect of variation in mean viscosity ($\bar{\mu}$) and its stratification on the short-term dynamics of the flow, we plot the contours of maximum temporal energy amplification on the wavenumber plane in Fig. 10. The Mach number, Reynolds number and reference Prandtl number considered are 5, 10^5 and 0.2 respectively. Figs. 10a, 10b and 10c represent the reference, μ-averaged, and μ-stratified flows respectively. The μ-averaged flow has a higher mean viscosity, which leads to a higher Prandtl number ($= 0.34$) in the flow, compared to the reference case ($Pr = 0.2$).

We observe that the initial energy of the disturbance in the reference flow amplifies significantly more compared to the other two flows (see Fig. 10). Increase in viscosity from 1 in the reference flow, to 1.7 in the μ-averaged flow, leads to a lower energy amplification in the case of averaged flow. The effect of viscosity stratification on transient energy amplification is obtained by comparing Fig. 10b with 10c, since both the flows have the same average value of viscosity. We notice that the stratification in viscosity reduces the energy amplification significantly, making it the least stable among these flows. It can be noted that the maximum energy amplification at all Mach and Prandtl numbers occurs for a spanwise disturbance ($\alpha = 0$), similar to the κ-varying flows discussed in section IV A. Ref. [22] reports similar effect of viscosity stratification on the maximum temporal growth of perturbation energy, but their work reflects coupled variation of conductivity and viscosity as well. It can be noted that the physical mechanism leading to the transient energy growth for the flow cases presented in Fig. 10 is again the lift-up mechanism.

To study the effect of viscosity stratification on the transient energy growth, Chikkadi et al. [16] study two types of channel flows. First one with shear-thinning fluids, and another case with two miscible fluids of same density, but different viscosities. Sameen et al. [17] consider a symmetrically as well an asymmetrically heated channel flow, and neglected Prandtl number and buoyancy, to isolate only the effect of viscosity stratification. Both the studies report that the disturbance kinetic energy amplification and the streamwise vortices are practically unaffected by viscosity stratification.

In conclusion, we note that for a compressible Couette flow, the stratification in viscosity has a dramatic stabilizing effect, compared to an increase in the mean viscosity value. This result is valid at finite time as well as asymptotic limits, irrespective of any Mach, Reynolds and Prandtl number of the flow.

C. Viscosity & conductivity stratification

Linear stability results in the Mach number-wavenumber plane

Figure 11a presents the reference flow ($\bar{\mu} = \bar{\kappa} = 1$) with the same reference Prandtl number as that of the μ-κ-stratified flow (Fig. 11d), in which viscosity and conductivity are varying independently as functions of temperature (see section II C). Figure 11b represents the μ-κ-averaged flow, with constant values of fluid viscosity ($= 2.6$) and thermal conductivity ($= 3$). These are representative values averaged over a range of Mach numbers from 0.1 to 20 for an equivalent μ-κ-stratified flow (at reference $Pr = 0.2$). Figure 11c is also an averaged flow, but in this case, the values of viscosity and conductivity at each Mach number are different. These are averaged values at each Mach number corresponding to the μ-κ-stratified flow shown in Fig. 11d.

The effect of increase in the magnitude of mean viscosity and conductivity is obtained by comparing the stability characteristics of Fig. 11a with 11b. We notice that both the flows have the same maximum disturbance growth rate ($= 0.05$), but an increase in the transport property values makes the averaged flow slightly more unstable compared to the reference case. The signature of the presence of stratification in both viscosity and conductivity on flow stability can be realized by comparing Fig. 11c with 11d, since both the flows have the same average values of conductivity and viscosity at each Mach number. We notice that most of the regions in the M-α plane is stable in the case of μ-κ-stratified flow (Fig. 11d), in contrast

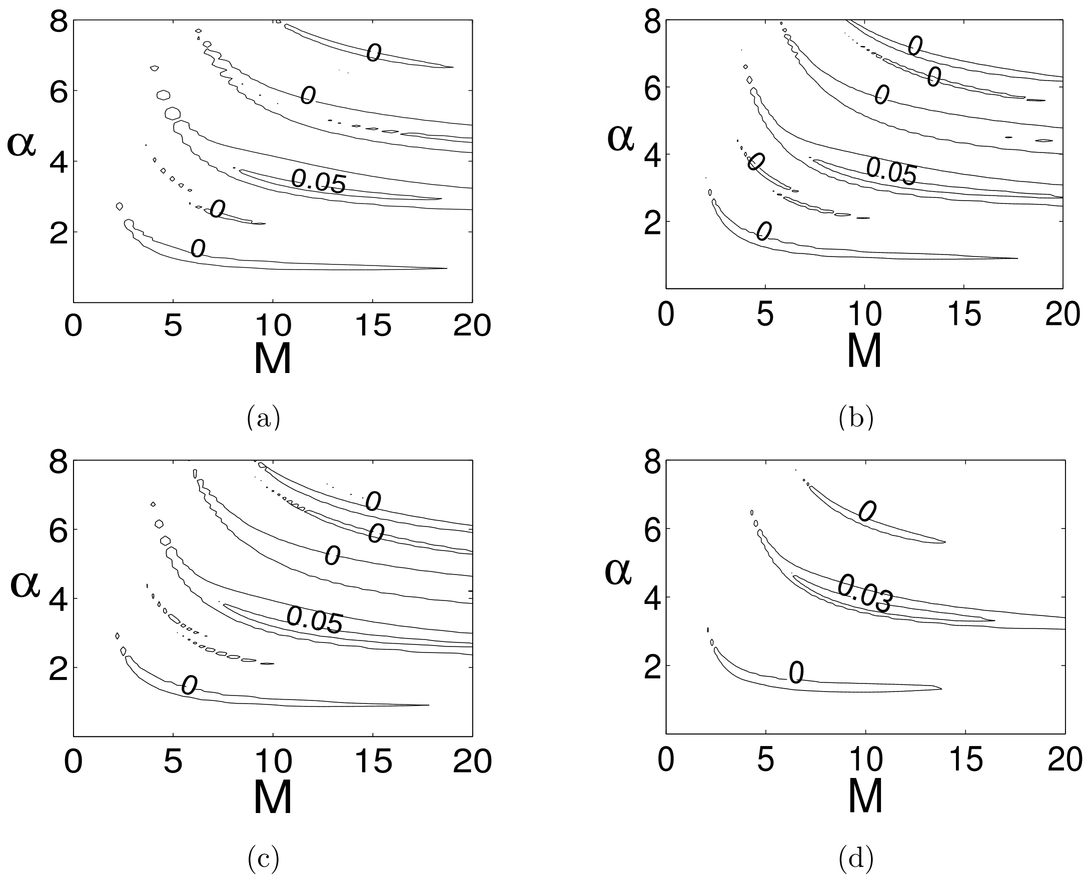

FIG. 11: Stability diagrams in the Mach-streamwise wavenumber plane for (a) the reference flow, (b) μ-κ-averaged flow with $\bar{\kappa}_{avg} = 3$ and $\bar{\mu}_{avg} = 2.6$, (c) μ-κ-averaged flow with $\bar{\kappa}_{avg}$ and $\bar{\mu}_{avg}$ varying with Mach number, and (d) μ-κ-stratified flow. Reference Prandtl number is 0.2, $\beta = 0$ and $Re = 10^5$.

to the μ-κ-averaged flow (Fig. 11c). In addition, there is a reduction in the maximum growth rate at comparable Mach and disturbance wave numbers. This implies that simultaneous stratification in $\bar{\mu}$ and $\bar{\kappa}$ has a stabilizing role. This is in line with our previous observation that viscosity stratification is strongly stabilizing, while variation in thermal conductivity has a minor effect on flow stability. In addition, conductivity stratification has a mixed effect of stabilizing or destabilizing depending on the Mach number and Prandtl number of the flow. Thus, the stability of Couette flows with simultaneous variations in viscosity and thermal conductivity is found to be dominated by the viscosity stratification effects, and this is further elucidated by the Re-α plots presented next.

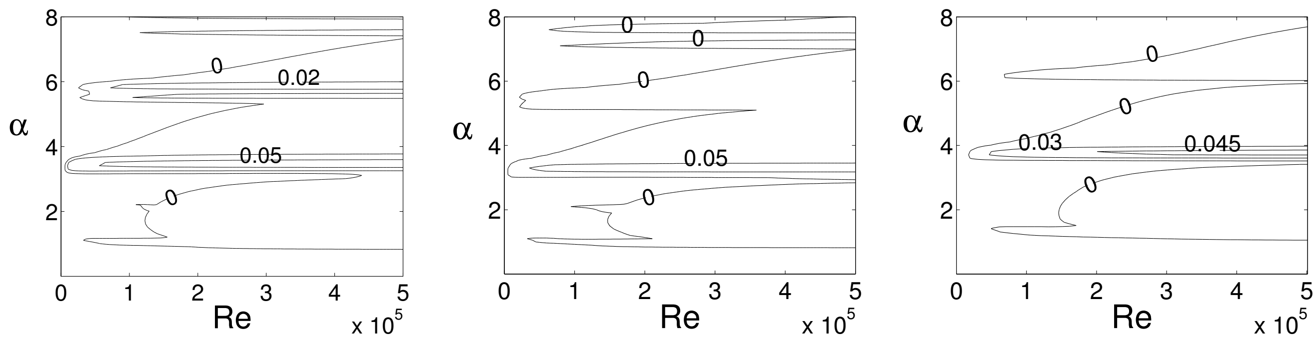

(a) (b) (c)

FIG. 12: Comparison of stability diagrams in the Reynolds number-streamwise wavenumber plane for (a) the reference flow, (b) μ-κ-averaged flow with $Pr_{avg} \approx 0.17$, (c) μ-κ-stratified flow. Reference Prandtl number considered is $Pr = 0.2$ and $M = 10$.

Stability analysis in the Reynolds number-wavenumber plane

Figure 12 presents the least stable growth rates in the Reynolds number versus wavenumber plane for three model Couette flows with different values of viscosity and conductivity. As earlier, the reference Prandtl number and Mach number considered are 0.2 and 10 respectively, and disturbances are assumed to be two-dimensional. The average Prandtl number for the μ-κ-stratified flow at $M = 10$ and $Pr = 0.2$ is around 0.17, which is the reference Prandtl number for the μ-κ-averaged flow.

Once again, the stability diagrams of the reference and μ-κ-averaged flow are similar in terms of the regions of instability and their growth rates (compare Figs. 12a and 12b). The critical Reynolds numbers listed in Table III at different Mach numbers show that the μ-κ-averaged flow is marginally unstable compared to the reference flow for all Mach numbers and at Prandtl numbers 0.72 and 0.2. The comparison of the critical wavenumbers predicts that the same instability loop (second loop in Fig. 12) contributes to the critical Reynolds number for both the flows.

Comparison of Fig. 12b with 12c shows that the stratification in both viscosity and conductivity decreases the maximum growth rate slightly, but the instability regions along the disturbance wavenumber axis decrease considerably. This stabilizing effect of $\bar{\mu}$ and $\bar{\kappa}$ stratification is more prominent at high reference Prandtl numbers, as can be observed from Table III. At Mach 5, for example, stratification in viscosity and conductivity increases the Re_{cr} by a factor of two for reference $Pr = 0.2$. The critical Reynolds number is enhanced by a factor of more than three for the same flow at $Pr = 0.72$. We notice that for all Mach and

TABLE III: Comparison of critical Reynolds number and wavenumber at various Mach numbers for three different model Couette flows, with varying viscosity and conductivity. Reference Prandtl numbers considered are 0.72 and 0.2.

		Re_{cr}				α_{cr}		
Pr	M	Reference	μ-κ-avg	μ-κ-strat	Pr_{avg}	Reference	μ-κ-avg	μ-κ-strat
0.72	3	40555	37323	111026	0.67	2.58	2.55	2.85
0.72	5	19527	17497	54115	0.63	2.18	2.10	2.57
0.72	10	36437	32333	131551	0.59	1.93	1.79	2.45
0.2	3	9704	9444	18316	0.194	2.43	2.43	2.24
0.2	5	10442	9488	18466	0.187	5.22	5.12	1.76
0.2	10	5232	4540	15840	0.174	3.34	3.17	3.70

Prandtl number combinations, the μ-κ-stratified flow has the maximum critical Reynolds number, while μ-κ-averaged flow has the least Re_{cr} value. *Therefore, in terms of the linear stability results, we can infer that the presence of stratification in viscosity and conductivity can delay flow transition considerably.*

Transient growth results

To investigate the effect of simultaneous variations in viscosity and conductivity on transient energy growth, we plot the contours of maximum temporal energy amplification in Fig. 13. The first three sets of figures (13a, 13b and 13c) are at a Mach number of 5, whereas the next three are shown for a higher Mach number of 10. The Reynolds number and reference Prandtl number considered are 10^5 and 0.2 respectively. A higher increase in conductivity compared to viscosity, for a given temperature profile, leads to a lower Prandtl number in the averaged flows, in comparison with the corresponding reference flows. The μ-κ-averaged flows with a Prandtl number of around 0.19 at $M = 5$ and 0.17 at $M = 10$ are shown in Figs. 13b and 13e respectively.

Similar to the previous transient growth results discussed in sections IV A and IV B, the maximum energy amplification for the reference and the μ-κ-averaged flow occur for a disturbance with $\alpha = 0$. However, in the case of μ-κ-stratified flow, transient energy

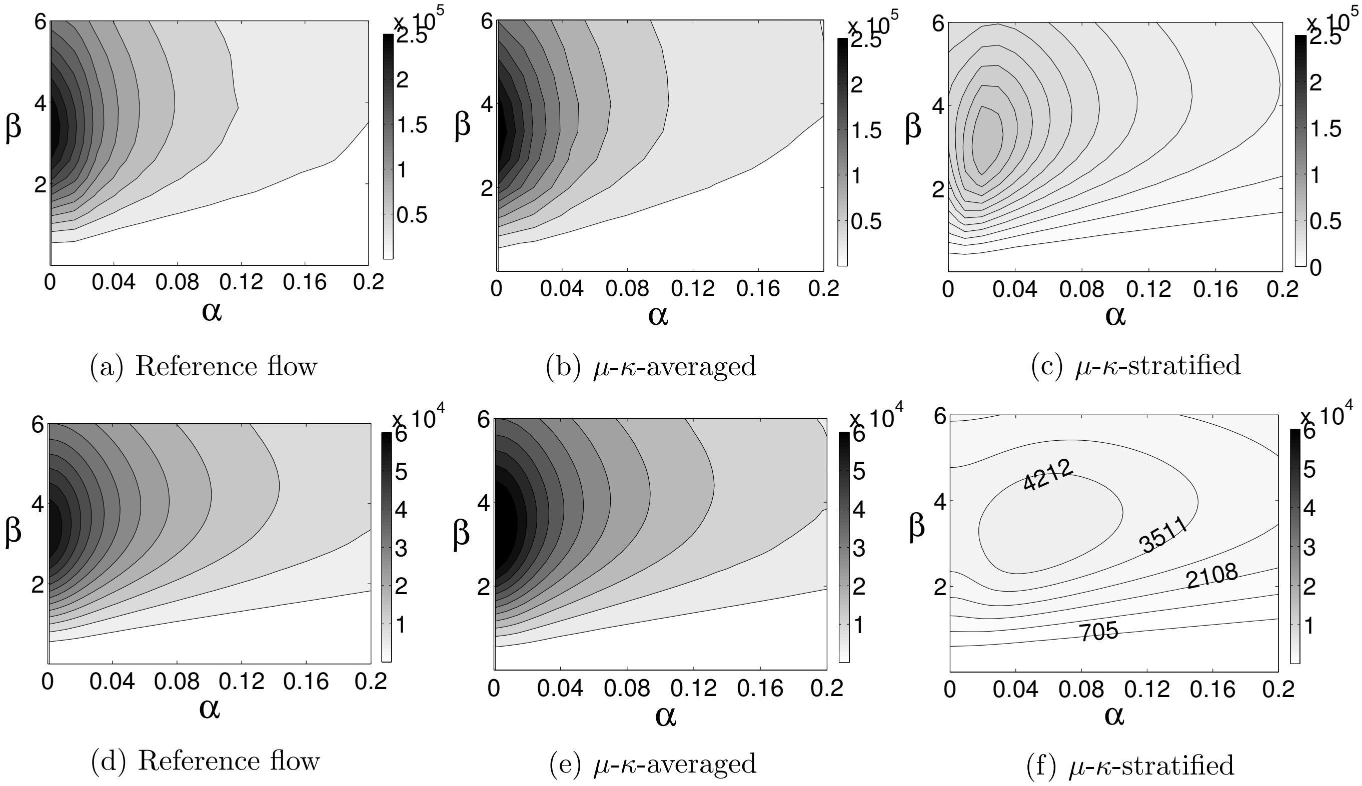

(a) Reference flow

(b) μ-κ-averaged

(c) μ-κ-stratified

(d) Reference flow

(e) μ-κ-averaged

(f) μ-κ-stratified

FIG. 13: Contours of maximum temporal energy amplification in the wavenumber plane showing the effect of stratification in viscosity and conductivity. Figures (a), (b) and (c) are at a Mach number of 5, while (d), (e) and (f) are plotted at $M = 10$. Here, $Re = 10^5$ and reference $Pr = 0.2$. Prandtl numbers corresponding to the averaged flows (b) and (e) are 0.187 and 0.174 respectively.

reaches a maximum value at finite streamwise and spanwise wavenumbers (see Figs. 13c and 13f). Therefore, the optimal disturbance is not streamwise independent or pure streamwise vortices. The optimal patterns are modulated vortices similar to the ones presented in Ref. [28], and are observed between a Mach number ranging from 2 to 14, for the Prandtl number considered here.

The transient growth analysis exhibits similar results of increase in $\bar{\mu}$ and $\bar{\kappa}$, and their stratification, as predicted by the linear stability theory. The disturbance energy amplification in the μ-κ-averaged flow (Fig. 13b) is found to be comparable to that in the reference flow (Fig. 13a). On the other hand, a simultaneous variation of viscosity and conductivity (Fig. 13c) shows significantly lower transient energy amplification than the μ-κ-averaged flow (Fig. 13b), with uniform transport properties maintained at the respective averaged values. Increasing the Mach number from 5 to 10, leads to a considerable decrease in the disturbance energy growth for all the three base flow cases considered, but the relative magnitudes between the reference, μ-κ- averaged, and μ-κ-stratified cases is identical to that at the lower Mach number.

It can thus be noted that, in a μ-κ-stratified flow, viscosity stratification plays a dominant role compared to the stratification in thermal conductivity. The destabilizing effect of increase in conductivity is overcome by the presence of stratification in viscosity, due to which μ-κ-stratified flow is far more stable compared to a flow with uniform transport properties.

In contrast to κ-stratified and μ-stratified flows, where the physical mechanism responsible for transient growth is the lift-up effect, in a μ-κ-stratified Couette flow both the lift-up effect and Orr-mechanism together decide the transient energy growth. The disturbances primarily gain energy using the vortex-tilting mechanism, but obtain an additional increment of growth due to the energy transfer from the mean flow, which occurs via the Reynolds stress and the coupling of the wall-normal velocity with temperature and density fluctuations due to compressibility. Contrary to optimal perturbations in a Couette flow with streamwise wavenumber $\alpha = 0$ (see Fig. 8c), the vortices in a μ-κ-stratified flow are not symmetrical about the wall-normal axis, but are tilted against the mean shear, and the energy is extracted from the mean shear by transporting momentum down the mean momentum gradient (through Orr-mechanism) while trying to rise to an upright position as time evolves. The optimal velocity disturbance pattern corresponding to the maximum transient amplification for a Couette flow with $\alpha_{opt} \neq 0$ is shown in Ref. [28], and is not repeated here.

The optimal structures observed in an incompressible Couette flow are similar to the ones presented here. For a constant shear incompressible Couette flow, Butler and Farrell [32] describe the physical mechanisms leading to the transient energy growth of two-dimensional and three-dimensional disturbances. Two dimensional perturbations with a favourable initial phase tilt opposite to the mean shear are found to exhibit rapid energy growth, due to the Reynolds stress or the Orr mechanism. However, amplification of the disturbance energy in this case is found to be lower than three-dimensional optimal disturbances, where the lift-up mechanism leads to the formation of streamwise rolls and streaks. Further, Butler and Farrell find that $3-$D optimal disturbances with non-zero α and β can lead to the highest transient energy amplification due to the interplay of both the vortex-titling and Reynolds stress mechanism. In a subsequent work, Farrell and Ioannou [33] study an unbounded constant shear flow of an incompressible fluid. They note that the main factor deciding the physical mechanism is the ratio of spanwise to the streamwise wavenumber ($r = \beta/\alpha$). Orr mechanism is present when $r = 0$ (i.e., $\beta = 0$), and the lift-up mechanism is observed in the limit of r tending to infinity ($\alpha = 0$). For the intermediate values of the wavenumber ratio, both the Orr and lift-up mechanisms are at work, and a great increase in the streamwise velocity streaks is observed due to the induction of strong cross-stream velocities by the Orr mechanism. Similar trends are observed in the viscosity and conductivity stratified compressible Couette flow, where intermediate values of r (α >0 and β >0) lead to the maximum transient energy amplification (see Figs. 13c and 13f).

D. Transient energy budget

In this section, we present a budget of the transient energy growth to get physical insight into the underlying processes. Total energy of the perturbation is decomposed into its constituents,

$$\frac{\partial E}{\partial t} = -i \int_0^1 \phi^+ \mathbf{M} B \phi \, dy + c.c. = \frac{\partial P}{\partial t} + \frac{\partial V}{\partial t} + \frac{\partial T}{\partial t} + \frac{\partial S}{\partial t} + \frac{\partial W}{\partial t}, \tag{20}$$

where B and $\mathbf{M}$ are defined in section III and c.c. denotes complex conjugate. Here, P represents the production of perturbation energy due to mean flow gradients, D is the dissipation due to viscous effects and T represents thermal diffusion. The work done by viscous shear is denoted by S and pressure work terms are included in W. These energy constituents are computed as per the expressions given in appendix 2, and are used to investigate the effect of variation in transport properties on these energy transfer mechanisms.

Figure 14 presents the budget of perturbation energy corresponding to the optimal disturbance ($\alpha = 0$ and $\beta = 3.6$) in the reference and κ-averaged Couette flows. The energy budget for the κ-stratified flow is almost identical to the κ-averaged case, and is not shown in the figure. The parameters considered here are same as in Figs. 7a and 7b, and the eigenvalues with a growth rate higher than -0.5 are used in budget computations. The constituent energies shown in Fig. 14 are integrated values across the shear layer. It is found that the production, dissipation and thermal diffusion (to a smaller extent) are the main contributors to the total energy. Their magnitudes increase monotonically in time and reach asymptotic values eventually. The trend is similar to that in Fig. 14a in Ref. [28], which is used to validate our methodology of budget computation. A balance between the

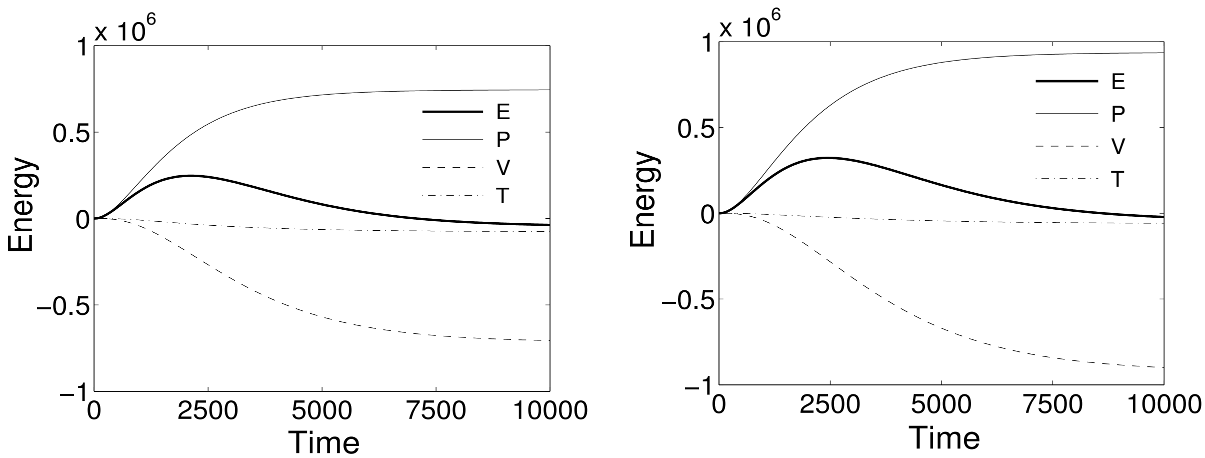

(a) Reference flow

(b) κ-averaged

FIG. 14: Comparison of energy budget for the reference and the κ-averaged flow corresponding to the maximum transient energy amplification in Fig. 7a and 7b respectively. Here E, P, V and T represent total energy, production or energy transferred from the mean flow, viscous dissipation and thermal diffusion respectively, and the variation of each term with time is shown.

constituent energies results in a net energy gain at short times and is shown by the bold solid line in Fig. 14. The shear work and energy transferred by the pressure forces are significantly less, and are not shown in the figure.

Comparing Fig. 14a with 14b we notice that the energy transferred from the mean flow to the disturbance is significantly higher in the case of κ-averaged flow compared to the reference case. The viscous forces play a significant role in the κ-averaged flow, and it leads to a higher energy lost by viscous dissipation compared to the reference flow. The energy transferred due to thermal diffusion is found to be negligible compared to the above two terms. The net effect of increased production and dissipation in the κ-averaged flow leads to an increase in the peak total energy by a factor of 1.3 compared to the reference flow. Also, the location of the peak energy shifts to a later time, denoting a longer duration of transient energy growth in the flow with higher thermal conductivity. Stratification of conductivity in the Couette flow is found to have comparatively small effect on the constituent energies, as noted earlier. The budget data thus shows that the increase in the magnitude of conductivity plays a major role in the redistribution of energy transferred from the mean flow to the disturbances. Hence the energy amplification factors in the κ-averaged flow presented in Fig. 7 are higher than the reference flow at comparable wave numbers.

The effect of stratification in viscosity on different constituents of perturbation energy is

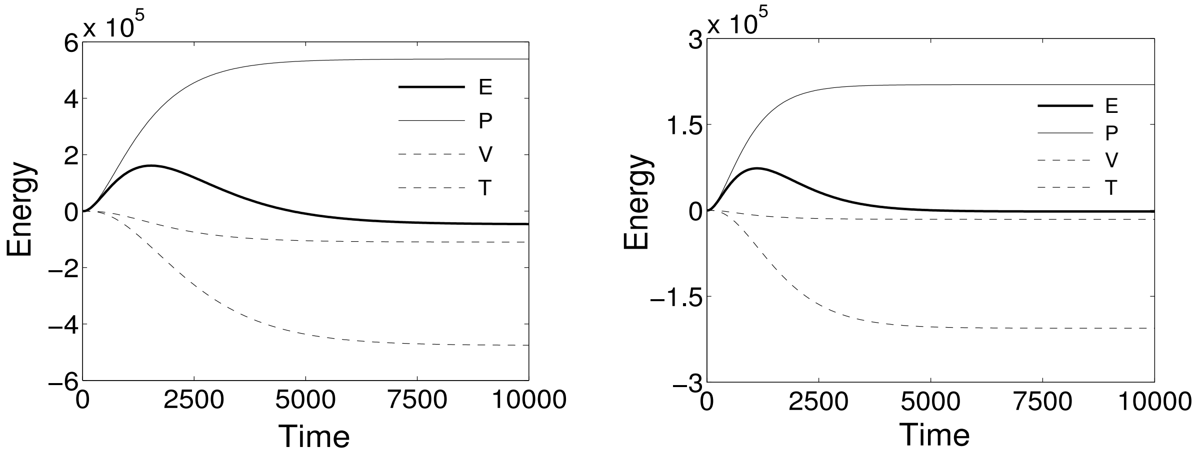

(a) μ-averaged (b) μ-stratified

FIG. 15: Comparison of energy budget for the total perturbation energy for the μ-averaged and the μ-stratified flow corresponding to the maximum transient energy amplification in Fig. 10b and 10c respectively.

presented in Fig. 15. We plot the energy budgets for the μ-averaged and the μ-stratified flow for parameters identical to those in Figs. 10b and 10c respectively. The data correspond to the optimal disturbances ($\alpha = 0$ and $\beta = 3.6$) that lead to the maximum transient energy amplification in each case. It is found that the peak total energy in a μ-stratified flow is around two times lower than the μ-averaged case. This can be attributed to a decrease in energy transfer from the mean flow to the disturbance, which is around 2.5 times less compared to the averaged flow. Stratification in viscosity also leads to a significant reduction in the energy lost by viscous dissipation and thermal diffusion. The decrease in magnitude of the total energy and its constituents leads to lower gain factors in the μ-stratified flow compared to the averaged flow (see Figs. 10b and 10c).

Next we analyze the combined effect of viscosity and conductivity stratification on various energy transfer mechanisms by comparing the energy budgets for a μ-κ-stratified flow with the corresponding μ-κ-averaged flow. Figure 16 plots the constituent energies corresponding to the base flow parameters in Fig. 13, for the wavenumber values which leads to the maximum transient energy amplification in each case. Comparison of Fig. 16b with 16a shows that in the case of μ-κ-stratified flow, all the energy transfer mechanisms have a sharp variation at small time, and rapidly approach their respective asymptotic values. The combined effect of viscous forces and thermal diffusion dissipates all the energy transferred from the mean flow, leading to a negligible value of the total energy beyond $t = 2000$. In

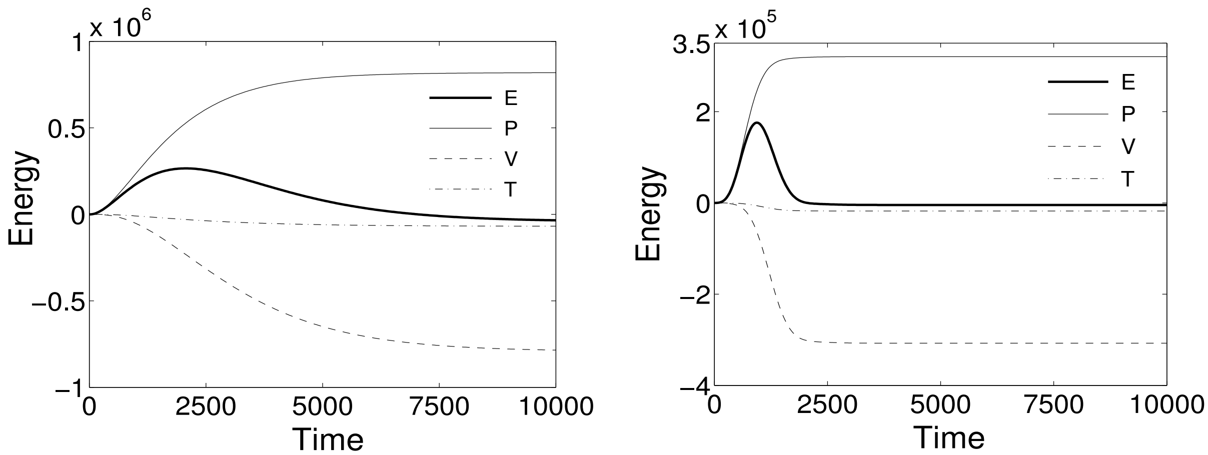

(a) μ-κ-averaged (b) μ-κ-stratified

FIG. 16: Comparison of energy budget for the total perturbation energy for the μ-κ-averaged and the μ-κ-stratified flow corresponding to the maximum transient energy amplification in Fig. 13b and 13c respectively.

the case of μ-κ-averaged flow we notice a gradual increase in the different constituents of total perturbation energy, and the peak in the total energy appears at a later time compared to the stratified case. Further, stratification in viscosity and conductivity also leads to a significant reduction ($\sim$ 2.6 times) in the energy intake from the mean flow, which causes less energy available to redistribute and dissipate by various physical energy transfer mechanisms. Overall, the stratified flow has significantly lower total energy content in the disturbance, as compared to the corresponding μ-κ-averaged flow. This is in line with our earlier finding that viscosity stratification effect dominate over conductivity effects, which leads to a smaller transient energy amplification in the case of μ-κ-stratified flow compared to the μ-κ-averaged flow, as seen from Fig. 13.

A similar budget analysis is performed for modal energy growth rate, by comparing the production, dissipation and thermal diffusion for the least stable eigen modes in the reference, μ-stratified and κ-stratified flows. The physical effects of transport property stratification are found to be in line with those presented above for non-modal energy budget, and the modal results are not reported separately, for the sake of brevity.

V. CONCLUSION

In realistic high Mach number flows, transport properties have large independent variations with temperature and pressure, which implies that they can not be related using a constant

Prandtl number. In this paper, we carry out a series of numerical experiments to isolate the effect of transport property variation on high-speed flow stability, using linear stability theory and transient growth analysis. For this, three different model Couette flows are considered, namely, the reference flow ($\bar{\mu} = \bar{\kappa} = 1$), flow with stratified viscosity and conductivity, and another flow where either viscosity, or thermal conductivity is varying, keeping the other constant across the shear layer. All the above flows are maintained at the same reference conditions. To isolate the effect of the gradients in transport properties from their magnitude, we define an equivalent uniform flow, with the same average values of transport properties as that of the corresponding stratified flow.

Temporal linear stability theory is applied for a large range of Mach numbers and Reynolds numbers, for different values of reference Prandtl number. Cases with Prandtl number varying across the shear layer are also considered. The growth rates of the most unstable eigenmode and the critical Reynolds number are reported for the different base flows. The results indicate a significant destabilizing role of increasing the mean conductivity value, while gradient in conductivity has a mixed stabilizing and destabilizing effect depending on the Mach and Prandtl number of the flow. By comparison, the gradient in viscosity has a strong stabilizing role at all Mach, Reynolds and Prandtl numbers. The stabilizing effect increases with Mach number, and it can lead to an order in magnitude increase in the critical Reynolds number. The simultaneous variation in viscosity and conductivity is also found to stabilize all the model flows considered in this work, where the physical effect of viscosity stratification dominates over that of the thermal conductivity variations.

To investigate the effect of transport properties on short time flow dynamics, we compute the maximum transient energy amplification for a wide range of disturbance wavenumbers and mean flow parameters. The Mack energy norm for compressible flows is used. Transient growth analysis reveals similar trends as predicted by the linear stability theory, namely, significant reduction in energy amplification due to the presence of viscosity gradients in the flow, and a considerable increase in the disturbance energy amplification for higher thermal conductivity of the fluid. In flows with either viscosity or conductivity stratification, the optimal transient energy gain is reached for $\alpha = 0$ i.e. streamwise independent disturbances. These are initially streamwise vortices that evolve in to low and high speed streaks in the streamwise velocity. This corresponds to the well-known lift-up effect, and results in alternating streaks of high and low temperature and density fluctuations. The perturbation energy is found to have a large temperature contribution, with appreciable exchange between the internal and the kinetic energy of the perturbations.

Simultaneous stratification of both viscosity and conductivity decreases the transient energy growth, and the extent of energy amplification decreases with increase in the Mach number. The optimal disturbance, in this case, has non-zero streamwise wavenumber; the vortical structures are not streamwise independent and are tilted against the mean shear. Both the lift-up effect and the Orr-mechanism together decide the transient energy growth.

To get a insight into the underlying physical processes leading to the transient energy growth, we present a non-modal energy budget for the total perturbation energy. The variation of constituent energies with time shows that the production, dissipation and thermal diffusion are the main contributors to the total disturbance energy. We find that both the energy transfer from the mean flow and the energy lost by viscous forces increase significantly with the increase in the conductivity value, leading to a higher transient energy gain in the κ-averaged flow. Stratification in viscosity has the opposite effect on the constituent energies, and results in a lower transient energy amplification. There is significant reduction in the production term when both viscosity and conductivity stratification is present in the flow, causing a smaller transient energy growth. In addition, the energy amplification occurs over a smaller time scale in μ-κ-stratified Couette flows.

Overall, the current work elucidates the individual and competing effects of momentum and thermal diffusivities on the stability of compressible Couette flow. The insight gained in this work, we believe, will provide useful input towards understanding the stability of complex high-speed flows.

Appendix 1

The linear stability equations for the perturbations can be expressed as an eigenvalue problem, which is,

$$B\psi = \omega I \psi, \tag{21}$$

This can be expanded as,

$$\begin{bmatrix} B_{11} & B_{12} & \dots & B_{15} \\ B_{21} & B_{22} & \dots & B_{25} \\ \vdots & & \dots & \vdots \\ \vdots & & \dots & \vdots \\ B_{41} & B_{42} & \dots & B_{45} \\ B_{51} & B_{52} & \dots & B_{55} \end{bmatrix} \begin{Bmatrix} \hat{u} \\ \hat{v} \\ \hat{w} \\ \hat{\rho} \\ \hat{T} \end{Bmatrix} = \omega \begin{bmatrix} 1 & 0 & \dots & 0 \\ 0 & 1 & \dots & 0 \\ \vdots & & \dots & \vdots \\ \vdots & & \dots & \vdots \\ 0 & 0 & \dots & 0 \\ 0 & 0 & \dots & 1 \end{bmatrix} \begin{Bmatrix} \hat{u} \\ \hat{v} \\ \hat{w} \\ \hat{\rho} \\ \hat{T} \end{Bmatrix} \tag{22}$$

The rows in the above system correspond to the x-momentum, y-momentum, z-momentum, continuity and energy equation respectively. The elements of the matrix B are:

$$B_{11} = \alpha\bar{u} - i\frac{\left[\bar{\mu}\left(\alpha^2+\beta^2\right) + \alpha^2\left(\bar{\mu}+\bar{\lambda}\right) - \bar{\mu}_y D - \bar{\mu}D^2\right]}{\bar{\rho}Re},$$

$$B_{12} = -i\bar{u}_y - \alpha\frac{\left[\bar{\mu}_y + \left(\bar{\lambda}+\bar{\mu}\right)D\right]}{\bar{\rho}Re},$$

$$B_{13} = -i\alpha\beta\frac{\left(\bar{\lambda}+\bar{\mu}\right)}{\bar{\rho}Re},$$

$$B_{14} = \frac{\alpha\bar{T}^2}{\gamma M^2},$$

$$B_{15} = \frac{\alpha}{\gamma M^2} + i\frac{\left[\bar{u}_{yy}\bar{\mu}_T + \bar{u}_y\bar{T}_y\bar{\mu}_{TT} + \bar{u}_y\bar{\mu}_T D\right]}{\bar{\rho}Re},$$

$$B_{21} = -\alpha\frac{\left[\bar{\lambda}_y + \left(\bar{\lambda}+\bar{\mu}\right)D\right]}{\bar{\rho}Re},$$

$$B_{22} = \alpha\bar{u} + i\frac{\left[\left(\bar{\mu}_y+\bar{\lambda}_y\right)D - \bar{\mu}\left(\alpha^2+\beta^2\right) + \left(\bar{\mu}+\bar{\lambda}\right)D^2 + \bar{\mu}_y D + \bar{\mu}D^2\right]}{\bar{\rho}Re},$$

$$B_{23} = -\beta\frac{\left[\bar{\lambda}_y + \left(\bar{\lambda}+\bar{\mu}\right)D\right]}{\bar{\rho}Re},$$

$$B_{24} = -i\frac{\left(\bar{T}_y + \bar{T}D\right)}{\bar{\rho}\gamma M^2},$$

$$B_{25} = -i\frac{(\bar{\rho}_y + \bar{\rho}D)}{\bar{\rho}\gamma M^2} - \frac{\alpha\bar{u}_y\bar{\mu}_T}{\bar{\rho}Re},$$

$$B_{31} = -i\alpha\beta\frac{\left(\bar{\lambda} + \bar{\mu}\right)}{\bar{\rho}Re},$$

$$B_{32} = -\beta\frac{\left[\bar{\mu}_y + \left(\bar{\lambda} + \bar{\mu}\right)D\right]}{\bar{\rho}Re},$$

$$B_{33} = \alpha\bar{u} - i\frac{\left[\bar{\mu}\left(\alpha^2 + \beta^2\right) + \beta^2\left(\bar{\mu} + \bar{\lambda}\right) - \bar{\mu}_y D - \bar{\mu}D^2\right]}{\bar{\rho}Re},$$

$$B_{34} = \frac{\beta\bar{T}^2}{\gamma M^2},$$

$$B_{35} = \frac{\beta}{\gamma M^2},$$

$$B_{41} = \alpha\bar{\rho},$$

$$B_{42} = -i\left(\bar{\rho}_y + \bar{\rho}D\right),$$

$$B_{43} = \beta\bar{\rho},$$

$$B_{44} = \alpha\bar{u},$$

$$B_{45} = 0,$$

$$B_{51} = \alpha\left(\gamma - 1\right)\bar{T} + i\frac{2\left(\gamma - 1\right)M^2\bar{\mu}\bar{u}_y D}{\bar{\rho}Re},$$

$$B_{52} = -i\bar{T}_y - i\left(\gamma - 1\right)\bar{T}D - \frac{2\alpha\left(\gamma - 1\right)M^2\bar{\mu}\bar{u}_y}{\bar{\rho}Re},$$

$$B_{53} = \beta\left(\gamma - 1\right)\bar{T},$$

$$B_{54} = 0,$$

$$B_{55} = \alpha\bar{u} + i\frac{\left[\bar{T}_{yy}\bar{k}_T + \bar{T}_y^2\bar{k}_{TT} + 2\bar{T}_y\bar{k}_T D - \left(\alpha^2 + \beta^2\right)\bar{k} + \bar{k}D^2 + \left(\gamma - 1\right)M^2\,Pr\,\bar{u}_y^2\bar{\mu}_T\right]}{\bar{\rho}\,Re\,Pr}.$$

Here, D is the differential operator; subscripts y and T denote the derivatives with respect to y and $\bar{T}$ respectively.

Appendix 2

The decomposition of total perturbation energy gives rise to production, viscous dissipation, thermal diffusion, shear work and pressure energy. The mathematical expression corresponding to the individual terms are mentioned below.

Production:

$$\frac{\partial P}{\partial t} = -\int_0^1 \left[\bar{\rho}\,\bar{U}_y\,u_s^+ v_s + \frac{\bar{T}}{\gamma M^2 \bar{\rho}}\,\bar{\rho}_y\,\rho_s^+ v_s + \frac{\bar{\rho}}{\gamma(\gamma-1)M^2\bar{T}}\,\bar{T}_y\,T_s^+ v_s\right] dy + c.c. \tag{23}$$

Viscous dissipation:

$$\begin{aligned}\frac{\partial V}{\partial t} = -\frac{1}{Re}\int_0^1 [&\alpha^2(\bar{\mu}+\bar{\lambda})\,u_s^+ u_s + \bar{\mu}(\alpha^2+\beta^2)\,u_s^+ u_s - u_s^+(\bar{\mu}_y\,D + \bar{\mu}\,D^2)u_s - i\alpha\bar{\mu}_y\,u_s^+ v_s \\ &-i\alpha(\bar{\mu}+\bar{\lambda})\,u_s^+ Dv_s + \alpha\beta\,(\bar{\mu}+\bar{\lambda})\,u_s^+ w_s - (\bar{U}_{yy}\,\bar{\mu}_T + \bar{U}_y\bar{T}_y\,\bar{\mu}_{TT})u_s^+ T_s - \bar{U}_y\bar{\mu}_T\,u_s^+ DT_s \\ &-i\alpha\bar{\lambda}_y\,v_s^+ u_s - i\alpha(\bar{\mu}+\bar{\lambda})\,v_s^+ Du_s + \bar{\mu}(\alpha^2+\beta^2)\,v_s^+ v_s - (\bar{\mu}_y+\bar{\lambda}_y)v_s^+ Dv_s - (\bar{\mu}+\bar{\lambda})\,v_s^+ D^2 v_s \\ &-\bar{\mu}_y\,v_s^+ Dv_s - \bar{\mu}\,v_s^+ D^2 v_s - i\beta(\bar{\mu}+\bar{\lambda})\,v_s^+ Dw_s - i\alpha\bar{U}_y\bar{\mu}_T\,v_s^+ T_s - i\beta\bar{\lambda}_y\,v_s^+ w_s - i\beta\bar{\mu}_y\,w_s^+ v_s \\ &+\alpha\beta(\bar{\mu}+\bar{\lambda})\,w_s^+ u_s - i\beta(\bar{\mu}+\bar{\lambda})\,w_s^+ Dv_s + \bar{\mu}(\alpha^2+\beta^2)\,w_s^+ w_s + \beta^2(\bar{\mu}+\bar{\lambda})\,w_s^+ w_s \\ &-\bar{\mu}\,w_s^+ D^2 w_s - \bar{\mu}_y\,w_s^+ Dw_s]\,dy + c.c\end{aligned} \tag{24}$$

Thermal diffusion:

$$\begin{aligned}\frac{\partial T}{\partial t} = \frac{\bar{\rho}}{\gamma(\gamma-1)\,Re\,Pr\,M^2}\int_0^1 [&\bar{\kappa}_T\,\bar{T}_{yy}\,T_s^+\,T_s + \bar{T}_y^2\,\bar{\kappa}_{TT}\,T_s^+\,T_s + 2\,\bar{T}_y\,\bar{\kappa}_T\,T_s^+\,DT_s \\ &-\bar{\kappa}\,(\alpha^2+\beta^2)\,T_s^+\,T_s + \bar{\kappa}\,T_s^+\,D^2 T_s]\,dy + c.c\end{aligned} \tag{25}$$

Shear work:

$$\frac{\partial S}{\partial t} = \frac{\bar{\rho}}{\gamma\,Re}\int_0^1 [2\,\bar{\mu}\,\bar{U}_y\,T_s^+\,Du_s + 2\,i\alpha\,\bar{\mu}\,\bar{U}_y\,T_s^+\,v_s + \bar{\mu}_T\,\bar{U}_y{}^2\,T_s^+\,T_s]\,dy + c.c \tag{26}$$

Pressure energy:

$$\frac{\partial W}{\partial t} = \frac{1}{\gamma\,M^2}\int_0^1 [p_s^+\,Dv_s + v_s^+\,Dp_s]\,dy + c.c \tag{27}$$

where, $p_s = \bar{\rho}\,T_s + \bar{T}\rho_s$

Appendix 3: Validation study

We have used Chebyshev spectral collocation method for discretization, and the results presented in the paper are grid converged. In this section, we carry out a validation study for the numerical method used in the paper by comparing with some of the previous work.

Figure 17 plots the eigenspectrum for a compressible Couette flow with uniform shear at $M = 2$, $Pr = 0.72$, $Re = 2 \times 10^5$ and $\alpha = \beta = 0.1$. The case corresponds to Fig. 2*b* of Ref. [28]. We notice a good match between our plot (Fig. 17a) and Fig. 2*b* in Ref. [28]. For the range of disturbance frequencies considered in Fig. 17a, first two acoustic modes are clearly visible in both the figures, and their respective growth rates match well. The **Y** shape of the viscous branch also compares well between the two figures.

In addition to this, we have also computed a case from Ref. 20 with parameters $M = 2$, $Pr = 0.72$, $Re = 2 \times 10^5$ and $\alpha = 0.1$. The results computed using 100 Chebyshev points match up to four decimal places with the data mentioned in Ref. 20.

The validation is also performed for transient energy growth calculation, where we compare the variation of energy amplification factor with time for a stratified viscosity and conductivity Couette flow at $M = 2$, $Pr = 0.72$, $Re = 2 \times 10^5$, $\alpha = \beta = 0.1$ (see Fig. 17b).

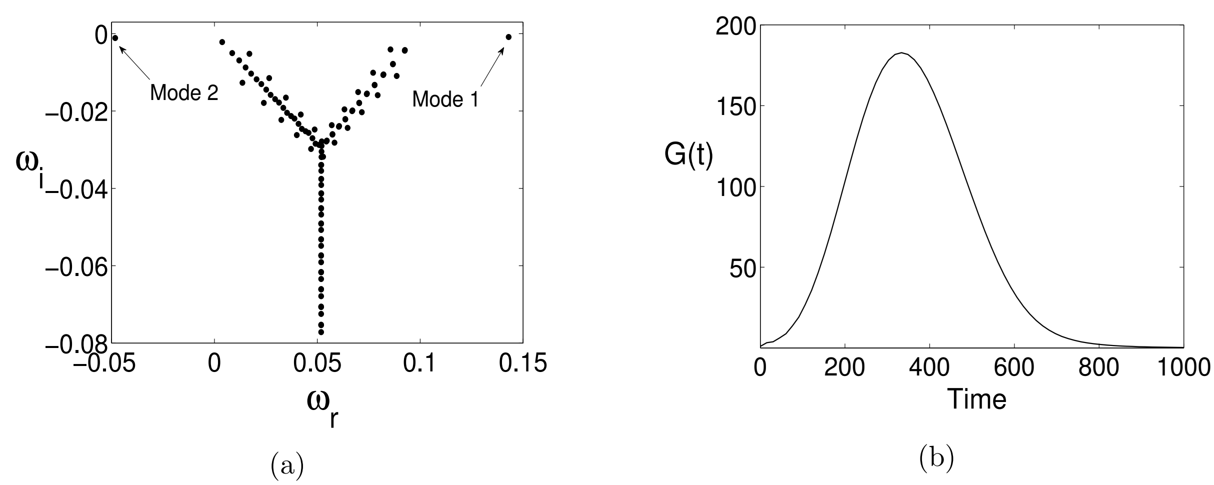

FIG. 17: (*a*) The eigenspectrum magnified near $\omega_r = 0$, for an uniform viscosity and conductivity compressible Couette flow at $M = 2$, $Pr = 0.72$, $Re = 2 \times 10^5$ and $\alpha = \beta = 0.1$. (*b*) Variation of the energy amplification factor, $G(t)$, with time for a viscosity and conductivity stratified Couette flow, with the same parameters as in (*a*).

A good match for the maximum energy amplification (~ 180) and the optimal time (~ 330) are found while comparing with Fig. 4a of Ref. [28].

---

[1] E. Reshotko, "Boundary-layer stability and transition," Annual Review of Fluid Mechanics 8 (1), 311, 1976.

[2] S. J. Leib, D. W. Wundrow and M. E. Goldstein, "Effect of free-stream turbulence and other vortical disturbances on a laminar boundary layer," Journal of Fluid Mechanics 380, 169, 1999.

[3] L. E. Ericsson, "Effect of nose bluntness and cone angle on slender-vehicle transition," AIAA journal 26 (10), 1168, 1988.

[4] P. S. Klebanoff and K. D. Tidstrom, "Mechanism by which a two-dimensional roughness element induces boundaryLayer transition," Physics of Fluids 15 (7), 1173, 1972.

[5] M. R. Malik and D. I. A. Poll, "Effect of curvature on three-dimensional boundary-layer stability," AIAA journal 23 (9), 1362, 1985.

[6] K. J. Franko, R. W. MacCormack and S. K. Lele, "Effects of chemistry modeling on hypersonic boundary layer linear stability prediction," AIAA Paper No. 2010-4601, 2010.

[7] I. J. Lyttle and H. L. Reed, "Sensitivity of second-mode linear stability to constitutive models within hypersonic flow," AIAA Paper No. 2005-889, 2005.

[8] C. Yih, "Instability due to viscosity stratification," Journal of Fluid Mechanics 27 (2), 337, 1967.

[9] D. P. Wall and S. K. Wilson, "The linear stability of flat-plate boundary-layer flow of fluid with temperature-dependent viscosity," Physics of Fluids 9 (10), 2885, 1997.

[10] L. E. Sorokin, "Stability of flow with the thermal conductivity depending linearly on the temperature," Fluid Dynamics 32, 309, 1997.

[11] A. D. D. Craik, "The stability of plane Couette flow with viscosity stratification," Journal of Fluid Mechanics 36 (2), 687, 1969.

[12] B. T. Ranganathan and R. Govindarajan, "Stabilization and destabilization of channel flow by location of viscosity-stratified fluid layer," Physics of Fluids 13 (1), 1, 2001.

[13] R. Govindarajan, V. S. L'vov and I. Procaccia, "Retardation of the onset of turbulence by minor viscosity contrasts," Physical Review letters 87 (17), 174501, 2001.

[14] R. Govindarajan, V. S. Lvov, I. Procaccia and A. Sameen, "Stabilization of hydrodynamic flows by small viscosity variations," Physical Review E 67 (2), 026310, 2003.

[15] R. Govindarajan, "Effect of miscibility on the linear instability of two-fluid channel flow," International Journal of Multiphase Flow 30 (10), 1177, 2004.

[16] V. Chikkadi, A. Sameen, and R. Govindarajan, "Preventing transition to turbulence: A viscosity stratification does not always help," Physical Review Letters 95, 264504, 2005.

[17] A. Sameen and R. Govindarajan, "The effect of wall heating on instability of channel flow," Journal of Fluid Mechanics 577, 417, 2007.

[18] C. Nouar, A. Bottaro and J. P. Brancher, "Delaying transition to turbulence in channel flow: revisiting the stability of shear-thinning fluids," Journal of Fluid Mechanics 592, 177, 2007.

[19] M. I. Boulos, P. Fauchais and E. Pfender, *Thermal plasmas* (Springer, New York, 1994), Vol. 1, pp. 265-321.

[20] S. Hu and X. Zhong, "Linear stability of viscous supersonic plane Couette flow," Physics of Fluids 10 (3), 709, 1998.

[21] P. W. Duck, G. Erlebacher and M. Y. Hussaini, "On the linear stability of compressible plane Couette flow," Journal of Fluid Mechanics 258, 131, 1994.

[22] M. Malik, J. Dey and M. Alam, "Linear stability, transient energy growth, and the role of viscosity stratification in compressible plane Couette flow," Physical Review E 77 (3), 2008.

[23] M. R. Malik and E. C. Anderson, "Real gas effects on hypersonic boundary-layer stability," Physics of Fluids A: Fluid Dynamics 3 (5), 803, 2013.

[24] M. L. Hudson, N. Chokani and G. V. Candler, "Linear stability of hypersonic flow in thermochemical nonequilibrium," AIAA journal 35 (6), 958, 1997.

[25] A. Hanifi, P. J. Schmid and D. S. Henningson, "Transient growth in compressible boundary

layer flow," Physics of Fluids 8 (3), 826, 1996.

[26] N. P. Bitter and J. E. Shepher, "Transient growth in hypersonic boundary layers," AIAA Paper No. 2014-2497, 2014.

[27] B. T. Chu, "On the energy transfer to small disturbances in fluid flow (Part I)," Acta Mechanica 1 (3) 215-234, 1965.

[28] M. Malik, M. Alam and J. Dey, "Nonmodal energy growth and optimal perturbations in compressible plane Couette flow," Physics of Fluids 18 (3), 034103, 2006.

[29] D. G. Lasseigne, R. D. Joslin, T. L. Jackson and W. O. Criminale, "The transient period for boundary layer disturbances," Journal of Fluid Mechanics 381, 89, 1999.

[30] A. Ramachandran, B. Saikia, K. Sinha and R. Govindarajan, "Effect of Prandtl number on the linear stability of compressible Couette flow," International Journal of Heat and Fluid Flow, 2016.

[31] D. Tempelmann, A. Hanifi and D. S. Henningson, "Spatial optimal growth in three-dimensional compressible boundary layers," Journal of Fluid Mechanics 704, 251, 2012.

[32] K M. Butler and B. F. Farrell, "Three-dimensional optimal perturbations in viscous shear flow," Physics of Fluids A: Fluid Dynamics 4 (8), 1637-1650, 1992.

[33] B. F. Farrell and P. J. Ioannou, "Optimal excitation of three-dimensional perturbations in viscous constant shear flow," Physics of Fluids A: Fluid Dynamics 5 (6), 1390-1400, 1993.